Materials & Design 212 (2021) 110183

Contents lists available at ScienceDirect

Materials & Design

journal homepage: www.elsevier.com/locate/matdes

Wearable electronic devices for glaucoma monitoring and therapy

Wanqing Zhang [a,b,c], Lingling Huang [d], Robert N. Weinreb [d], Huanyu Cheng [b,*]

[a] James Watt School of Engineering, University of Glasgow, Glasgow, UK
[b] Department of Engineering Science and Mechanics, The Pennsylvania State University, Pennsylvania, USA
[c] Glasgow College, University of Electronic Science and Technology of China, Chengdu 611731, China
[d] Hamilton Glaucoma Center, Shiley Eye Institute and Viterbi Family Department of Ophthalmology at the University of California, San Diego, La Jolla, CA, USA

HIGHLIGHTS

- This work summarizes the recent advancement of wearable electronic devices for glaucoma monitoring and therapy.
- Electronics innovations with stretchable materials or structures have resulted in improved device performance.
- The monitoring devices with reduced power consumption and footprint demonstrate enhanced sensitivity, sensing distance, and measurement range.
- The drug delivery systems showcase sustained and self-adaptive drug release with enhanced efficiency.

GRAPHICAL ABSTRACT

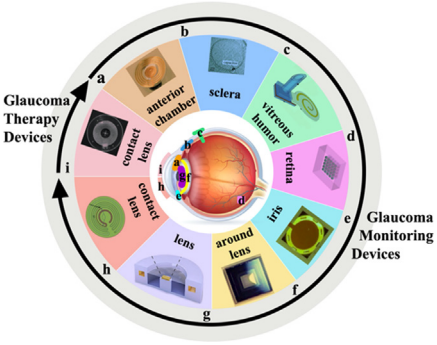

ARTICLE INFO

Article history:
Received 28 October 2020
Revised 3 May 2021
Accepted 16 October 2021
Available online 18 October 2021

Keywords:
Glaucoma monitoring and therapy
Intraocular pressure (IOP)
Drug delivery devices
Wearable electronic devices
Biomarker detection

ABSTRACT

Glaucoma is a leading cause of irreversible blindness worldwide, which is estimated to affect approximately 112 million people by 2040. Elevated intraocular pressure (IOP) is the most important risk factor for glaucoma, as well as the primary target for the treatment. Current therapies aim at IOP reduction to prevent the disease progression. The accurate and real-time measurement of IOP is therefore critical to evaluate treatment response and guide medical decisions. However, IOP fluctuates throughout the 24-hour cycle with different patterns from day to day in the same individual and also different patterns among individuals. The current clinical practice typically captures a single IOP measurement during "in-office hours", and this is insufficient for disease monitoring. With the development of wearable electronic devices, a variety of IOP monitoring devices provide a unique potential for continuous IOP monitoring. In addition to IOP monitoring for glaucoma management, this mini-review also summarizes novel drug delivery devices for treating glaucoma. Because certain types of glaucoma do not show elevated IOP, we also discuss the potential to incorporate biomarker detection with IOP measurement for more accurate and reliable glaucoma diagnostics and therapies.

1. Introduction

Glaucoma is a group of eye diseases associated with various pathophysiological processes that share a common endpoint of optic nerve damage [1]. Primary open-angle glaucoma (POAG) is

* Corresponding author.
E-mail address: Huanyu.Cheng@psu.edu (H. Cheng).

https://doi.org/10.1016/j.matdes.2021.110183
0264-1275/

the most common form of glaucoma and accounts for 70%-90% of the diseases [2]. As the leading cause of irreversible blindness worldwide, it is estimated that glaucoma will affect 112 million people by 2040 according to the World Health Organization [3]. Elevated intraocular pressure (IOP) is the most important risk factor and thus IOP monitoring is essential for glaucoma management [4].

Among various methods for IOP measurement, Goldmann applanation tonometry (GAT) is considered the gold standard. It requires specialized equipment operated by a trained professional. The Goldmann applanation tonometer measures the force required to flatten an area of the central cornea of 3.06 mm diameter. The accuracy of measurements is affected by the central corneal thickness, corneal edema, excessive or insufficient fluorescein dye in the tear film, high astigmatism, irregular or scarred cornea, Valsava maneuver or excessive external pressure on the eyelid. The IOP measured with Goldmann applanation tonometry represents a single time point during office hours, and this does not reliably represent a complete view of IOP due to the variability of IOP throughout the day and among days [56]. It is known that 24-hour IOP pattern in $\sim$ two thirds of individuals has a nocturnal peak during sleep and gradually decreases during the day [7–9]. Studies have shown that the peak IOP in glaucoma patients was recorded outside of office hours [10] and the peak IOP during 24-hour monitoring was significantly higher than the peak clinic IOP [11]. These findings highlight the urgent need of continuous real-time IOP monitoring to guide clinic decisions.

Minimally invasive implantable devices for IOP monitoring are usually placed at different intraocular locations, whereas non-invasive IOP monitoring devices often embed a pressure sensor in a contact lens or directly use the entire contact lens as the pressure sensor. One of these devices measures the change in corneal curvature and that measurement is then converted to an approximate IOP [12]. Other IOP monitoring devices measure the eye pressure by detecting changes in capacitance, inductance, color, or liquid displacement, corresponding to IOP changes. While elevated IOP remains the most significant risk factor for glaucoma, other factors, such as vascular diseases, also contribute to glaucoma pathophysiology. Studies have explored glaucoma-related biomarkers in the tear film or other biofluids to complement IOP measurements to better understand the pathophysiology of glaucoma.

Glaucoma leads to irreversible vision loss, but early effective treatment can slow down or even prevent further vision loss. The mainstay of treatment includes IOP-lowering eyedrops, laser surgery and incisional surgeries. Eyedrops are often used as the first line treatment given the effectiveness in IOP reduction and patient preferences. However, patient compliance with eyedrop administration is a major limiting factor to achieve optimal treatment effect [13]. In one study, 64% of glaucoma patients reported ocular discomfort caused by medications as the main contributor of non-compliance and 57% of patients reported difficulties in administering eye drops. Many patients are not aware of the importance of glaucoma treatment since there are usually minimal symptoms even in moderately advanced stages of the disease. Consequently, noncompliant patients are subject to a higher risk of irreversible optic nerve damage. By the time that the visual symptoms are appreciated by patients, considerable irreversible damage often is present. In order to improve patient compliance and the effectiveness of treatment, there is increasing interest in the idea of delivery devices to administer ocular medications on-demand.

The significant need for continuous glaucoma monitoring and drug delivery have catalyzed an interest in wearable electronic devices. In this mini-review, we first summarize and discuss the characteristics of various IOP monitoring devices and biomarker detection devices, including implantation sites, fabrication materials, and design structures. Next, we review the recent advancement of several representative drug delivery devices for glaucoma therapy. We then conclude with current challenges and provide perspectives for future developments toward accurate diagnostics and effective treatment of glaucoma.

2. Continuous glaucoma monitoring devices

The normal IOP has an average of 15.5 mmHg with a fluctuation of about 2.75 mmHg in a range from 10 to 21 mmHg [51], whereas the fluctuation in the glaucomatous eye can be up to 15 mmHg [52]. In response to 3 μm change of human corneal curvature over a typical radius of 7.8 mm, the IOP would change by 1 mmHg [53]. The pressure of greater than 21 mmHg (or 2.8 kPa) often indicates glaucoma [54]. In addition to high pressure sensitivity for minimized pressure offset drift [55], the IOP sensors also need to have a large range of detection, low limit of detection (2 mmHg [56]), proper sensing distance and frequency response (0–30 Hz [57]), and biocompatibility. The other considerations may also include device dimension, transparency, power consumption, and ease of removal.

Because of the ocular structure, various IOP monitoring sensors can be either minimally invasive or non-invasive. The structure of the ocular globe can be divided into two main parts – the anterior and posterior segments. The anterior portion includes the cornea, aqueous humor, conjunctiva, iris, ciliary body, and lens, occupying about one-third of an eye. The posterior portion consists of the choroid, retina, sclera, optic nerve, among others. Because the accuracy of IOP monitoring may be affected by ocular structure (e.g., sclera and corneal rigidity [5859]), the implantation location needs to be carefully evaluated. Many minimally invasive IOP monitoring devices are inserted in the anterior chamber (Fig. 1**a**) through the corneal incision. The available implantation space is about 3–4 mm in length and 12.5 mm in width [6061]. With pressure measurement independent from corneal rigidity and ocular surface, the sensors implanted in the anterior chamber often have their coil disk carefully designed to fit the width of the iris rim, which easily aligns with the reader coils. The implantation in front of the iris also allows for the largest sensing area without the obstruction of the trabecular meshwork. In contrast, implantation in the sclera (Fig. 1**b**) enhances the efficiency of inductive coupling by reducing energy absorption by the tissue. Another method is to only penetrate the needle inside the vitreous humor, with the other parts of the sensor left outside of the sclera (Fig. 1**c**). On the other hand, implantation onto the retina (Fig. 1**d**) can directly measure pressure near the optic nerve head (ONH) area. With the surface topology consisting of numerous folds, iris can accommodate mechanical deformations to allow for attachment needed for certain monitoring sensors (Fig. 1**e**). Moreover, the pressure sensor can be embedded in a capsular tension ring-like structure. After insertion into the eye during the cataract surgery along with the intraocular lens (IOL) (Fig. 1**f**), the capsular tension ring can expand the capsular bag and stabilize the lens. A more recent modification of this device is placed in the suprachoroidal space and was given FDA Breakthrough designation on April 28, 2021. Alternatively, pressure sensors can be directly integrated on the artificial IOL (Fig. 1**g**) to measure IOP. Additionally, the integration of the IOP sensor on a contact lens or direct use of the contact lens itself as a pressure sensor results can be employed to develop a non-invasive monitoring device (Fig. 1**h**). IOP monitoring devices have been applied to various implantation sites (Table 1), with different sensing performance characteristics.

2.1. Minimally invasive IOP monitoring devices

The working principle of capacitive IOP sensors is mainly based on the deflected diaphragm caused by the pressure change, which

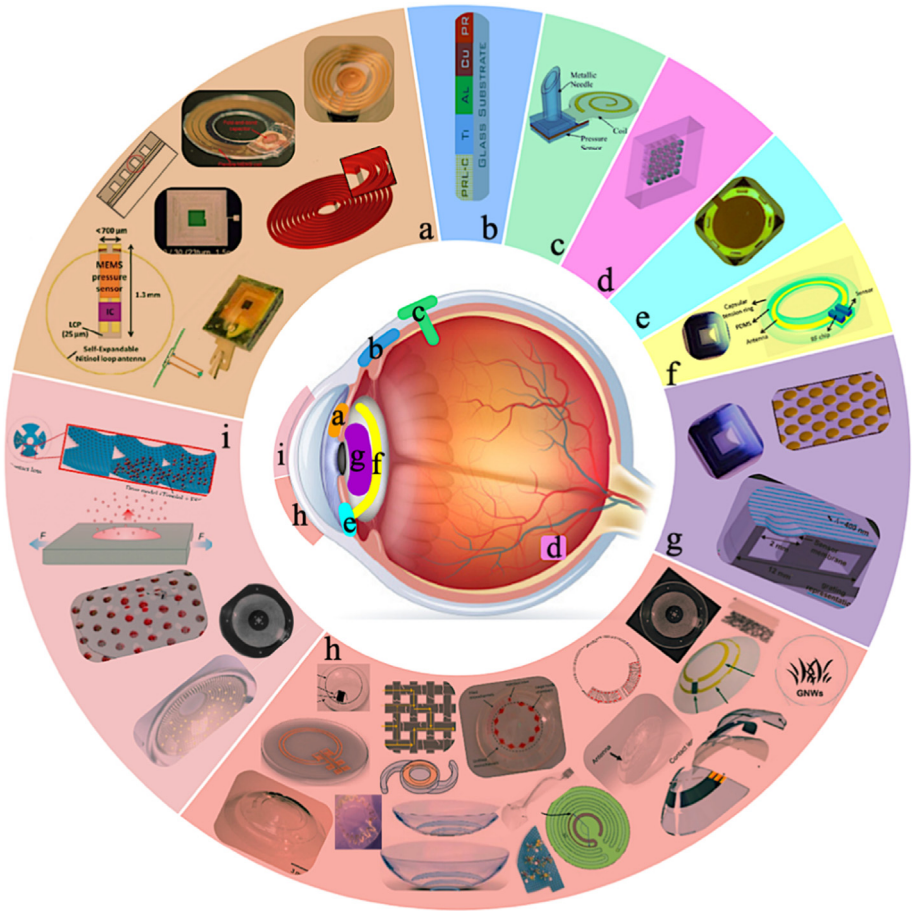

Fig. 1. A schematic to show the glaucoma monitoring and drug delivery devices (color-coded based on the locations). The sites of implant for minimally invasive intraocular pressure (IOP) sensors include (**a**) anterior chamber, reproduced with permission from [14–21], (**b**) sclera, reproduced with permission from [22], (**c**) inside the vitreous humor through penetration, reproduced with permission from [23], (**d**) retina, reproduced with permission from [24], (**e**) iris, reproduced with permission from [25], (**f**) around the lens, reproduced with permission from [26,27], and (**g**) lens, reproduced with permission from [27–29]. Non-invasive devices include (**h**) a set of non-invasive IOP sensors, reproduced with permission from [30–47], and (**i**) drug delivery devices for glaucoma therapy based on the contact lens, reproduced with permission from [37,38,48–50].

Table 1
Characteristics of various implantation sites for IOP devices.

Type	Implantation site	Feature	Ref
Minimally invasive IOP devices	Anterior chamber	Easy alignment with read coils; Large sensing area without obstruction of the trabecular meshwork	[14–21]
	Sclera	Reduced energy absorption by the tissue	[22]
	Vitreous humor	Reduced invasive space and achievable retrieval, if needed	[23]
	Retina	Direct pressure measurement	[24]
	Iris	Attachability with sensors	[25]
	Around the lens	Expanded capsular bag; stabilized lens	[2627]
	Lens	Direct artificial intraocular lens embedded	[27–29]
Non-invasive IOP devices	Contact lens	Pressure sensor embedded contact lens/pressure sensitive contact lens	[30–47]

results in the distance and then capacitance change. Injectable into the anterior chamber, a miniaturized micro-sensor for IOP monitoring consists of a CMOS IC, a self-expandable Nitinol antenna, and a MEMS capacitive pressure sensor (Fig. 2**a**) [14]. Different from rigid Si substrates, the liquid crystal polymer (LCP) of 25 μm as the soft substrate has been used for device fabrication for minimized damage to eye tissues. Because a thin Ti/Au electrode with a thickness of less than 1 μm is sandwiched by biocompatible parylene layers using parylene to parylene bonding, the overall thickness can be reduced from 100 μm (using sacrificial photoresist) to 30 μm, leading to a significantly enhanced flexibility. The sensor is attached to an epoxy mold with a radius of 5 mm for mimicking the bottom of the anterior chamber of the mouse eye (radius of more than 4 mm) *ex vivo*. In comparison to the high sensitivity of 0.75 fF/mmHg from the 100 μm-thick sensor ($500 \times 500 \times 100\ \mu m^3$), the miniaturized micro-sensor ($300 \times 300 \times 30\ \mu m^3$) still exhibits a sufficiently high sensitivity of 0.3 fF/mmHg to measure IOP change of 1 mmHg. To increase the capacitance value for easy measurement, the coil and capacitive pressure sensor can be fabricated on the polyimide substrate with a hollow mesa structure that comprises of a set of vertical windows (i.e., $20 \times 20 \times 20\ \mu m^3$ cavity) for increased capacitance (Fig. 2**b**) [15]. Served as additional capacitors, these windows help increase the capacitance by about five times on average. The device shows a linear measurement in the range from 10 to 21 mmHg with a sensitivity of 0.12 pf/mmHg *in vivo*. The minimally invasive implantation into the anterior chamber is achieved through a 1 mm scoring.

Because most RF powered devices implanted in the anterior chamber are floating, the alignment issue often occurs to result in a change in the amount of power transferred between the RF

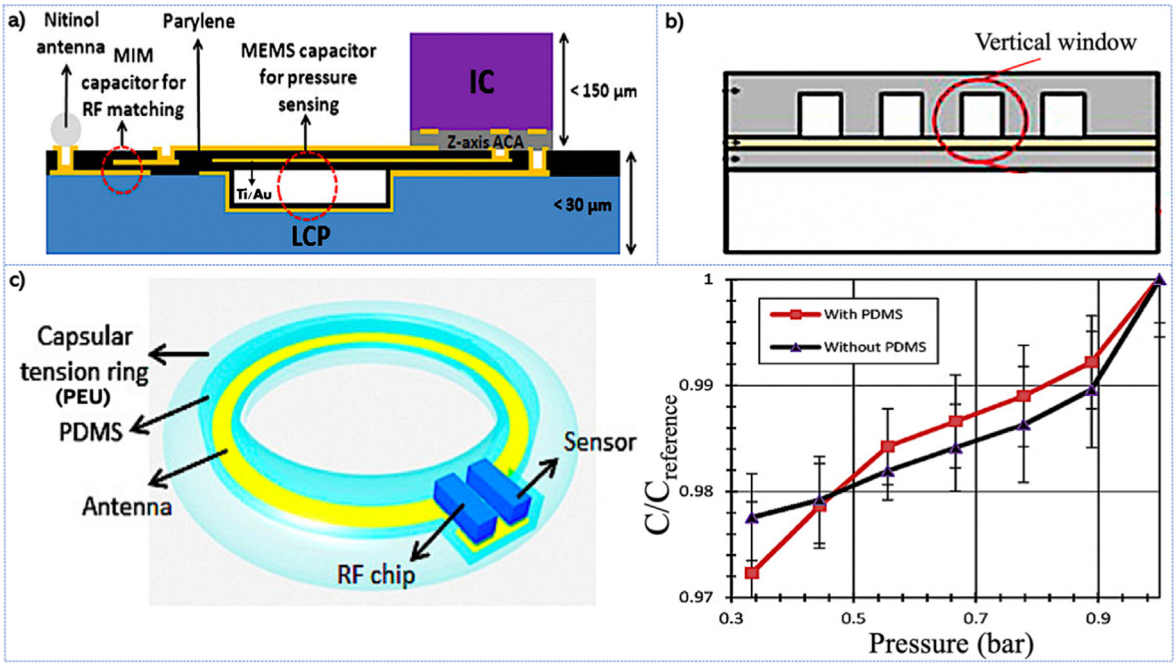

Fig. 2. Minimally invasive implantable capacitive pressure sensors. (a) The reduced thickness with the Ti/Au electrode sandwiched between parylene layers leads to enhanced flexibility of a miniatured micro-sensor (300x300 μm^2), which allows for easy injection into the anterior chamber with minimized tissue damage. Reproduced with permission from [14]. **(b)** A capacitive pressure sensor with a hollow mesa structure comprising of a set of vertical windows ($20 \times 20 \times 20\ \mu m^3$ cavity) is associated with capacitance increase by about five times. Reproduced with permission from [15]. **(c)** The flexible IOP device embedded into a capsular tension ring can be implanted during cataract surgery through a 2–3 mm incision using an injector. Permanent implantation is possible because of poly (ether urethane) (PEU) and polydimethylsiloxane (PDMS) barrier layers. Reproduced with permission from [26].

transmitter and devices. As one solution to address this issue, a prototype of a capacitive pressure sensor is embedded into a capsular tension ring-like structure with the implanted ring fixed. In addition to a capsular tension ring-like structure fabricated with poly (ether urethane) (PEU), this IOP device also includes an RF chip and an antenna packaged by flexible PDMS (Fig. 2**c**) [26]. Because of the increased parasitic capacitance (from 18.28 to 20.93 pF) from the PDMS coating, the average sensitivity increases from 0.60 to 0.69 pF bar^{-1} (0.80 to 0.92 fF/mmHg), with an upward shift in capacitance at all pressure levels. Although the first test with PCB embedded in PDMS indicates a failure below the benchmark of 50 kPa due to the weak adhesion between the surface mount technology component and antenna, the second test with the integrated circuit directly in the PDMS (i.e., without PCB components) highlights the flexible antenna that remains functional after 50 bending cycles under 116 kPa mechanical stress. Acted as barriers to prevent direct contact between the device components (i.e., chip and antenna) and the eye environment, PEU and PDMS layers can provide the device with an expected working lifetime of more than 50 years for a permanent implant.

Besides direct measurements, the capacitive sensors can also be used with the resonant-frequency measurements through a resistance-inductance-capacitance (RLC) or LC resonant circuit. IOP-induced frequency shift can be measured by an external reader through a wireless inductive coupling link. The resonant sensors may employ a variable capacitor or inductor as the pressure-sensitive element. As an example, a resonant sensor consisting of a variable capacitor integrated into a deformable diaphragm chamber and a flexible spiral inductor coil disk on a parylene C substrate is implanted into the anterior chamber with a small incision of less than 2 mm (Fig. 3**a**) [16]. The high yield strain of ~ 3% of parylene C allows the disk to recover back to its initial shape even after folding, without damage or permanent deformation in the unvaried inductance. The test with a live rabbit eye model reveals a pressure sensitivity of 455 ppm/mmHg with 1 mmHg resolution and responsivity of 160 kHz/mmHg (to detect phase-dip shift). However, the lossy medium in the anterior chamber results in the degraded quality factor from ~ 45 in water to ~ 6 in saline. As a result, the sensing distance is decreased from 25 mm in water to 15 mm in saline. This is attributed to the aqueous humor in the anterior chamber with high loss tangent for the reduced quality factor and sensing distance. To address this issue, the follow-up work attaches an implantation tube to the sensor's backside pressure access hole (Fig. 3**b**) [17]. By only inserting the tube into the anterior chamber, the sensing part attached to the cornea is exposed to air all the time, which minimizes the invasive surgery and maintains a quality factor of 27–30 in the sensor. As a result, the sensing distance can also be maintained at 25 mm. Tested by the analyzer, this improved IOP sensor has a sensitivity of 542 ppm/mmHg with a responsivity of about 205 kHz/mmHg.

Other than the novel sensor design to leave the sensing part exposed to the air, it is also possible to improve the sensing distance with a large coil dimension or a different design structure. The former can increase the coil dimension to about 15 mm in outer diameter (the variable capacitor sensing element based on a rigid, elliptical SU-8 structure), which allows for a large telemetry distance of 28 mm in deionized water (Fig. 3**c**) [18]. Although it is large in dimension, minimally invasive implantation can be achieved by rolling it through a small and self-healing corneal incision. Furthermore, the large capacitor chamber and several thin channels in the SU-8 structure connected to the capacitor chamber can provide an additional volume to the pressure reservoir to allow greater deflections for maximized pressure sensitivity. Though the device shows a high sensitivity of 156 kHz/mmHg using the impedance phase dip technique measured by an HP 4191A impedance analyzer, it is only for a small applied pressure and its linearity also needs to be improved. The latter strategy on the coil structure may explore a multipath circular spiral inductor consisting of three

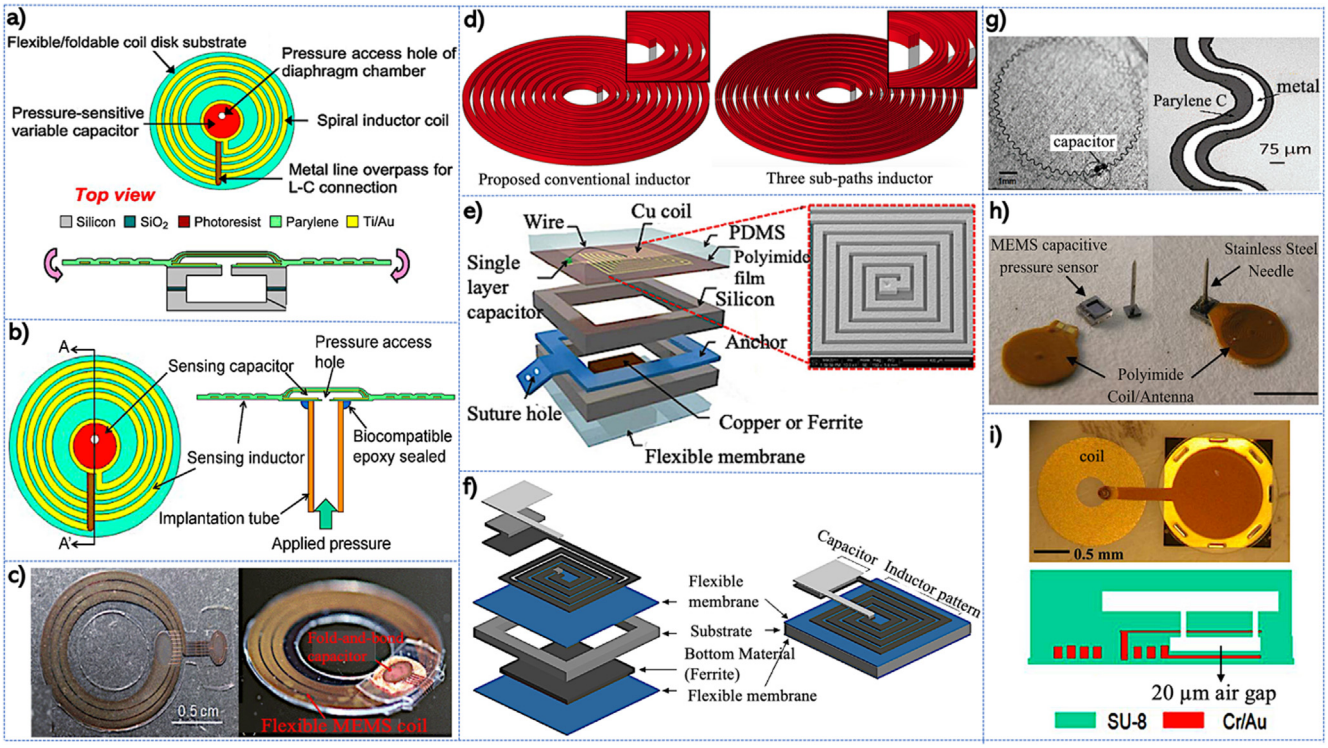

Fig. 3. Minimally invasive implantable pressure based on the detection of the resonant frequency shift. (a) A resonant sensor with parylene C substrate can be inserted into anterior chamber through incision of less than 2 mm. Reproduced with permission from [16] **(b)** With an implantable tube inserted into the anterior chamber, the 30 μm -thick parylene-based sensing part can attach to the cornea to achieve the minimally invasive implantation. Reproduced with permission from [17]. **(c)** The sensor with a unique pressure reservoir and an increased coil dimension to about 15 mm in outer diameter exhibits increased sensing distance and improved sensitivity. After the sensor is tightly rolled and implanted into the anterior chamber through a small, self-healing corneal incision, it can occupy the largest area without obstructing the trabecular meshwork, which results in a working distance of over 15 mm for the anterior chamber depth less than 3.5 mm. Reproduced with permission from [18]. **(d)** The sensor with three parallel sub-paths inductors exhibits enhanced Q factor without increasing dimension, which is suitable for the micro-scale implantation into the anterior chamber. Reproduced with permission from [19]. **(e)** A wireless inductive sensor consists of a bottom part inserted into the anterior chamber for pressure sensing (inductance change) and a top part fixed to the sclera for wireless data transfer. Reproduced with permission from [20]. **(f)** A ferrite magnet based inductive sensor enhances the resolution by using two flexible membranes in inductor pattern and ferrite material, which can be inserted into the anterior chamber. Reproduced with permission from [21]. **(g)** A wireless sensor with an integrated planar stretchable variable inductor can be implanted in the sclera to directly measure strain with reduced tissue energy absorption. Reproduced with permission from [22]. **(h)** With a hypodermic needle penetrated in the vitreous space, the device with most parts externally on the sclera achieves minimally invasive implantation and easy retrieval. Reproduced with permission from [23]. **(i)** The iris implanted resonant sensor with Au spiral coil inductor and capacitor exhibits improved sensitivity and increased Q factor. Reproduced with permission from [25].

sub-paths inductors (with unchanged path width) for the enhanced quality factor of the implanted sensor in the anterior chamber (Fig. 3**d**) [19]. The Au multipath inductor and variable capacitor decrease the coil series resistance and contribute to a high Q factor of 79, leading to a large sensing distance of 21 mm with a small footprint of 2.5 × 2.5 mm^2. The performance compares favorably against the other literature reports (e.g., Q factor of 30 with 3.23 × 1.52 mm^2 [23], or Q factor of 5.5 with 10 × 10 mm^2 [62]). The sensor also shows a relatively linear response with a sensitivity of 4281 ppm/mmHg in a pressure range of 0–60 mmHg using COMSOL Multiphysics and ADS software. Because of the use of SU-8 as the encapsulation material, the resulting device is biocompatible to prevent damage to eye tissue.

Although the variable-capacitor IOP sensors are widely used due to their high sensitivity and lower power consumption, they usually require a complicated MEMS process and the pressurized reference chamber may also lead to signal shift (3.47 mmHg of drift on average [63]). Besides, the significant degradation of phase depth in an aqueous environment reduces the signal strength in a wireless sensing system [16]. To address these issues, variable inductive sensors have been explored. In one example, a passive pressure sensor with inner materials (copper or ferrite) achieves a robust phase depth with high sensitivity (Fig. 3**e**) [20]. The top part of the sensor includes a micro-coil on a polyimide film and a capacitor, whereas the bottom part has a flexible membrane and an inner material. The bending of the flexible membrane upon IOP changes the distance between the micro-coil and inner material with the latter to affect the operational mechanisms of the sensor. With copper as inner material, the eddy current effect-based sensor requiring highlights a high sensitivity but without stable phase depth, irrespective of membrane sickness. In comparison, the sensor with inner ferrite material is based on the modulation of effective permittivity, highlighting stable phase depth but at the expense of sensitivity. This thin membrane (~60 μm) ferrite inductive sensor with a sensitivity of 1610 (or 1340) ppm/mmHg and phase depth of 3.37–3.49 (or 2.78–4.85) in ambient air (or *in vivo*) compares favorably over their capacitive counterparts of 455/0.4–0.5 [16] and 238/2.4 [23] (or 0.35 [16] and 0.28 [23] *in vivo*). As another method to enhance the sensing resolution, a spiral inductor and a moveable ferrite magnet with flexible membranes are fabricated (Fig. 3**f**) [21]. Although the simulation reveals a dynamic range of 0–70 mmHg, the eddy current generated on the cornea surface would degrade magnetic coupling between the IOP device and external coil to results in a reduced quality factor. Unlike the sensors with reference chambers, a variable inductor sensor without a sealed chamber eliminates the baseline drifts over time for long-term measurements with enhanced accuracy (Fig. 3**g**) [22]. Consisted of a planar variable inductor in a stretchable 'S-shape' and a commercial constant capacitor, the sensor implanted in the sclera can directly measure the strain with

reduced energy absorption from the tissue to enhance the efficiency of inductive coupling. Because of the unfolding of the stretchable coil, the sensitivity to measure the change of corneal curvature is enhanced to 57 kHz/mmHg in the test on a pig eye using an impedance analyzer *ex vivo* (though nonlinear). With a parylene-oil-encapsulation method, the sensor also shows low drift and long-term IOP monitoring capabilities when tested on rabbit *in vivo*, compared to a commercial pressure sensor (STMicroelectronics LPS25H) [64].

Because most of existing IOP pressure sensors are nondegradable, it is highly desirable to achieve minimally invasive implantation and the potential for retrieval after use, if needed. With a 30 gauge hypodermic needle penetrated inside the vitreous space, the rest of the sensor (e.g., capacitor and coil antenna on flexible polyimide) is left externally on the sclera surface for easy retrieval after monitoring **(**Fig. 3**h)** [23]. After a sensitivity of 15 kHz/mmHg with a resolution of 1 mmHg determined *in vitro*, a month of continuous monitoring *in vivo* also confirms its excellent biocompatibility. An iris implanted resonant sensor comprised of a planar spiral coil inductor, a capacitor with two parallel plates, and a SU-8 pressure-sensitive diaphragm also achieves relatively high sensitivity with an enhanced impedance phase dip frequency shift **(**Fig. 3**i)** [25]. The good sensitivity in the desired range of 0–60 mmHg results from the use of 18 μm-thick SU-8 membrane and a 20 μm gap to maximize its deflection. Compare to the literature reports (i.e., 102 kHz/mmHg [65] and 160 kHz/mmHg [66] in air), the sensor showcases a high sensitivity of 7035 ppm/mmHg (or 1083 kHz/mmHg) in air and 3770 ppm/mmHg (or 683 kHz/mmHg) in saline. The use of 9 μm-thick Au with enhanced conductivity increases the quality factor and then improves the phase dip for a sensing distance up to 6 mm. It should be noted that the biocompatible issues of Si make it less attractive compared with other MEMS materials (i.e., SiO_2, SiN, Au, and SU-8 [6768]) despite its favorable mechanical characteristics and stable chemical properties. In particular, SU-8 has high biocompatibility with no apparent sign of tissue damage or inflammatory reaction [69], which is promising for minimally invasive wearable devices.

Optical sensing approaches for IOP monitoring include visual-identification, interferometry, fluorescence, or those to be detected by an external optical reader. Based on the surface plasmon of metal 2D gratings, a power-free IOP sensor aims to be inserted onto the retina to directly measure pressure near the optic nerve head area **(**Fig. 4**a)** [24]. Because of the inhomogeneous IOP throughout the eye and the key role of the accommodation process in the onset of glaucoma [70], it is vital for this sensor to measure the accommodative IOP spikes to facilitate the understanding of the pathophysiology of glaucoma. Small IOP change can be directly observed from the visible color shift (i.e., structural color in the visible range) in nanophotonic gratings embedded in an elastomeric material, as observed in the finite difference time domain simulation with IOP in the range of 0–50 mmHg. Another color-sensing optical strain sensor based on spectral reflectance can potentially be embedded into an artificial lens **(**Fig. 4**b)** [28]. With a high refractive index layer of TiO_2 nanoparticles on a periodically nanostructured PDMS membrane, the pressures can be calculated from the intensity change of the green color channel. The obtained limit of detection of 160 Pa or 1.2 mmHg is comparable to that of Goldmann tonometer (213 Pa or 1.6 mmHg). During the test, the position of the green center line can help determine the orientation of the device because it moves upon eye movements. The nanostructured area can also calibrate the device.

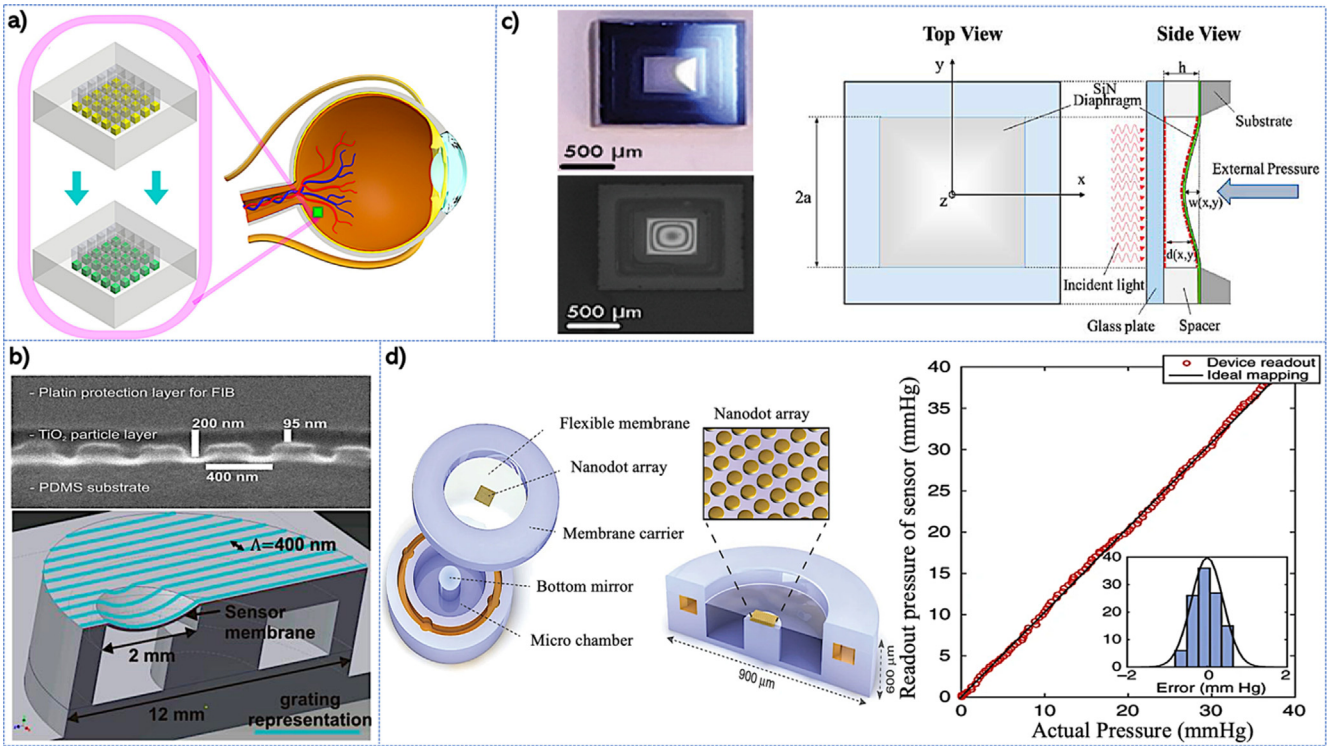

Fig. 4. Minimally invasive implantable optical pressure sensors. (a) A 2D plasmonic grating-based sensor aims to be implanted onto the retina near the optic nerve to directly measure stain near the optic nerve head in visible color change. Reproduced with permission from [24]. **(b)** A sensor based on the deformation of a photonic crystal (PC) waveguide with color change for potential integration into an artificial lens. Reproduced with permission from [28]. **(c)** An interferometric sensor with interference fringes between the diaphragm and glass substrate detected under monochromatic light (left). This sensor with a small form factor (1.5x1.5x0.4 mm^3) can be embedded into an intraocular lens or a capsular tension ring. Reproduced with permission from [27]. **(d)** A microscale sensor with enhanced optical resonance from the pressure-sensitive resonant cavity that has gold nanodots on the SiN membrane. With a size three orders of magnitude smaller than commercially available devices, this sensor can be inserted in an intraocular lens during cataract surgery or silicone haptics through a small cornea incision (decreased from 3 to 4 mm to 1–2 mm). Reproduced with permission from [29].

With a flexible 200 nm-thick silicon nitride diaphragm separated by a 10 μm-thick SU-8 spacer from a glass substrate to form a cavity, the interferometric pressure sensor can detect a small IOP change of 0.2 mmHg with a portable handheld reader (Fig. 4**c**) [27]. After the monochromatic light is directed to the sensor cavity, the interference fringes between the SiN diaphragm and the glass substrate resulted from the pressure change can be detected. Because of its small form factor (1.5x1.5x0.4 mm^3), this sensor can be inserted into an intraocular lens to cover only a small part or into the capsular tension ring to be implanted during cataract surgery. In comparison to a sensitivity of 31 nm/mmHg and an accuracy of 0.3 mmHg in a range of 0–60 mmHg *in vitro*, the *ex vivo* test still shows good accuracy of 0.6 mmHg in the range of 5–45 mmHg. Although the incident light is perpendicular to the sensor surface in the test, it may vary in real applications. A follow-up study with a two-stage bonding method for enhanced visibility of the interference fringes further confirms the biocompatibility and demonstrates its readout capability [71]. After replacing the CMOS camera and objective lens with a digital single-lens reflex camera and a macro lens in the handheld reader, the devices exhibit a sensitivity of 30 nm/mmHg and an accuracy of 0.2 mmHg in the range of 0–60 mmHg *in vitro*. The excellent biocompatibility is confirmed after ten-week implantation without any observable inflammation, biofouling, or signs of infection in the rabbits. As another interferometric device, the fiber-optical Fabry-Perot pressure sensor can also be integrated into the artificial cornea to monitor IOP in real-time for the use in keratoprosthesis [72].

Building on a prior work that explores a nanoscale textured surface (black-silicon/nanograss) to improve the biocompatibility [73], a microscale optical sensor with a nanodot-enhanced cavity can monitor IOP rapidly with high sensitivity and large sensing distance (Fig. 4**d**) [29]. Mounting the pressure sensors onto the intraocular lens (IOL) or silicone haptics minimizes the invasive damage during implantation. The sensor mounted on IOL can take advantage of the well-developed cataract surgery, whereas the one on silicone haptics requires a smaller corneal incision. Because the latter decreases the distance between the corneal surface and sensor from 3 to 4 mm to 1–2 mm, the signal-to-noise ratio increases from 12 to 15 dB. Compared to its RF-based counterparts with limited sensing distance, this device utilizes the invisible near-infrared light with little or nearly no loss in the tissue. The infrared light is used to detect the resonance of the pressure-sensitive cavity comprising of a micromachined silicon ring, a solid bottom Si surface, and a deformable top SiN membrane with a gold nanodot array for enhanced optical resonance. The device with a diameter of 900 μm is almost one order of magnitude smaller than sensors based on LC coupling and three orders of magnitude smaller than their commercial counterparts [63]. In addition to the high accuracy of 0.29 mmHg in the range of 0–40 mmHg with a large sensing distance of 30–50 mm (possibly beyond 100 mm) tested on equipment, the device also exhibits an accuracy of 1.3 mmHg *ex vivo* and continuous measurement up to 4.5 mon *in vivo*, as well as a rapid measurement of less than 1 s.

2.2. Non-invasive IOP monitoring devices

Thanks to the rapid advancement in biotechnology, microelectronics, and information technology, an electronic contact lens with integrated electrochemical and other sensors provides a promising platform for noninvasive monitoring and ocular diagnostics [7475]. Contact lens-based IOP sensor measures curvature changes of contact lens from the cornea radius variations (e.g.,

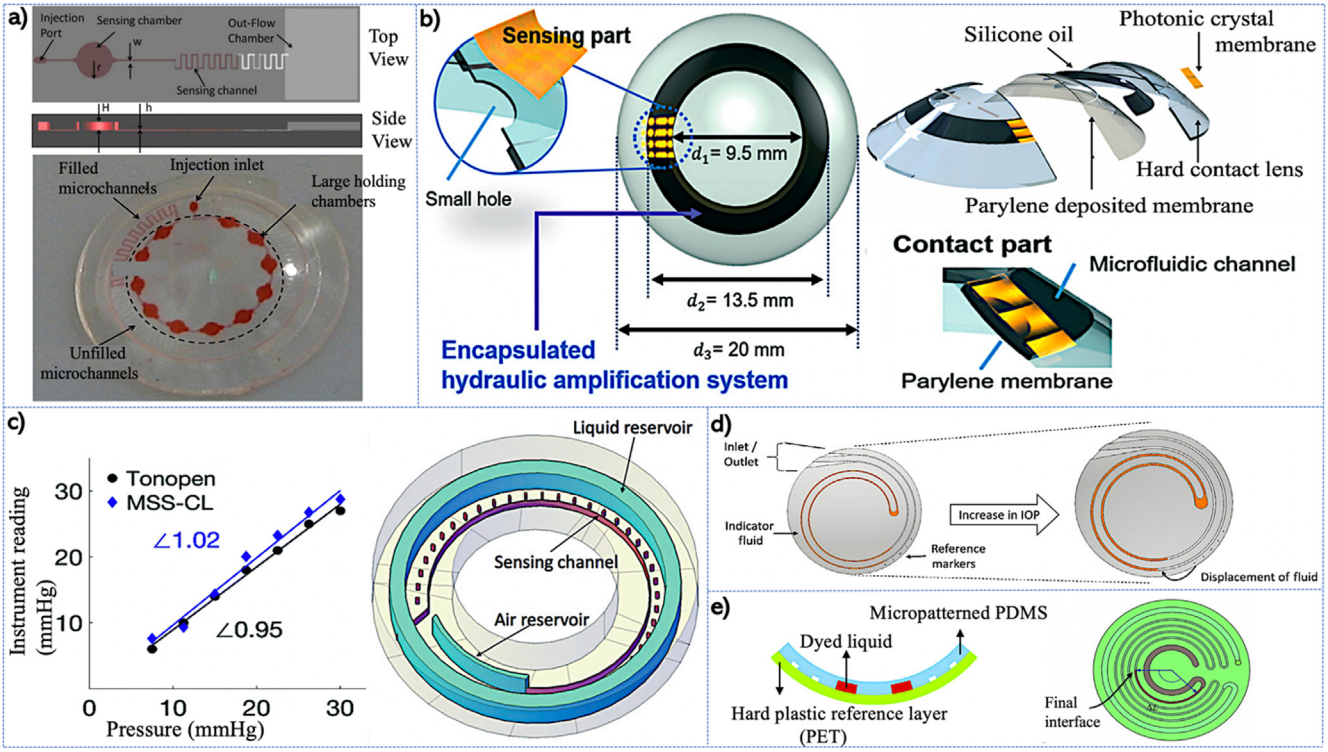

Fig. 5. Non-invasive microfluidic contact lens pressure sensors. **(a)** A microfluid contact lens sensor composed of a circular sensing chamber and sensing channels for amplified displacement upon pressure. As sensing channel width decreases, sensitivity is increased at the cost of dynamic range for a total length of 6 mm. Reproduced with permission from [30]. **(b)** A colorimetric IOP sensor with PC membrane fabricated by opal nanostructures and a microhydraulic amplification system for enhanced sensitivity. Reproduced with permission from [31]. **(c)** A silicone/hydrogel contact lens-based sensor uses a novel microfluidic dilatometer as the strain sensor and an oleophobic material NOA65 to eliminate oil absorption. Reproduced with permission from [40]. (**d**) A PDMS-based contact lens sensor with a double spiral-shaped microchannel to monitor IOP from the fluid displacement in the channel. The increased initial channel volume in the spiral-shaped design reduces the error in tracking fluid location. Reproduced with permission from [41]. **(e)** A microfluidic contact lens with a micropatterned soft elastomer sensing layer and a hard-plastic reference layer. The increased length of the chamber or decreased sectional area of the sensing channel enhances the sensitivity. Reproduced with permission from [42].

3 μm change of corneal curvature corresponding to 1 mmHg fluctuation in IOP) [76]. Compared to silicone with high air permeability, the silicone/hydrogel counterpart with enhanced water content improves wearing comfortability. Despite the extensive efforts, energy supply and wireless data transmission are still challenging. Methods for energy supply include battery [77], wireless power transfer (WPT), and wireless energy harvesting. The limited battery lifetime results in regular replacement. Although the energy can be transmitted inductively between coils through the magnetic field in WPT, the output power is constrained to 0.5–2 W [78]. As a result, a wirelessly rechargeable solid-state supercapacitor has been embedded into a contact lens for long-term use [79]. The wireless power harvesting system can also scavenge various energy forms, including motion, thermal and ambient RF energies. For instance, the system with a loop antenna, a rectifier, and an impedance matching network can convert the RF energy into a DC power with an RF-to-DC conversion efficiency of 35% at 5.8 GHz [80] (higher than 10% at 0.8–2 GHz [81]). As for wireless data transmission, the antenna as one of the most important components in different shapes (e.g., stretchable S shape, dipole shape, circular spiral shape, and single-loop shape) needs to be carefully designed [82]. The good mechanical compliance of the device can also be ensured with stretchable structures or materials, such as hybrid Ag nanofibers and nanowires for 30% biaxial tensile strain over 300 cycles.

A powerless microfluid pressure sensor can be directly embedded in a gas permeable hard contact lens with excellent oxygen permeability (Fig. 5**a**) [30]. Together with a large and tall circular sensing chamber network, the device also includes arrow and short sensing channels with each channel as an individual surface sensing element. In addition to the PDMS polymeric membrane and sensing surface, glycerol is also used to prevent fluid evaporation from PDMS. The magnitude of fluid displacement monitors the IOP, with the pressure difference at each contact point measured by the individual surface sensing element. As the sensing channel width increases (e.g., 20, 40, 80, 160 μm) for a total length of 6 mm, the sensitivity is decreased (600, 285, 130, 70 μm/mmHg), but the dynamic range is increased (10, 21, 46, 85 mmHg). Another hard contact lens-based sensor that integrates a microfluidic channel system with a PC membrane can monitor IOP from visual color change because the lattice distance in nanostructures changes with the deformation of corneal curvature (Fig. 5**b**) [31]. In addition to opal nanostructures integrated into a flexible and thin PDMS-based membrane, this colorimetric sensor also uses a microhydraulic amplification (with a parylene-coated ring-shaped fluidic channel) to enhance the range of color change for improved sensitivity. After optimizing the area ratio of two membranes to 1.5 mm hole size for the sensing part and 2.0 mm channel width for the contact part, the deformation of the sensor can be maximized. The device exhibits a sensitivity of 0.23 nm/mmHg in the range of 10–60 mmHg in the test *ex vivo*.

A silicone/hydrogel contact lens-based sensor can also use a microfluidic dilatometer as the strain sensor such that subtle changes of strain are converted into large fluidic volume expansion to be detected by a smartphone camera (Fig. 5**c**) [40]. However, the performance of the image-based strain sensor often deteriorates to

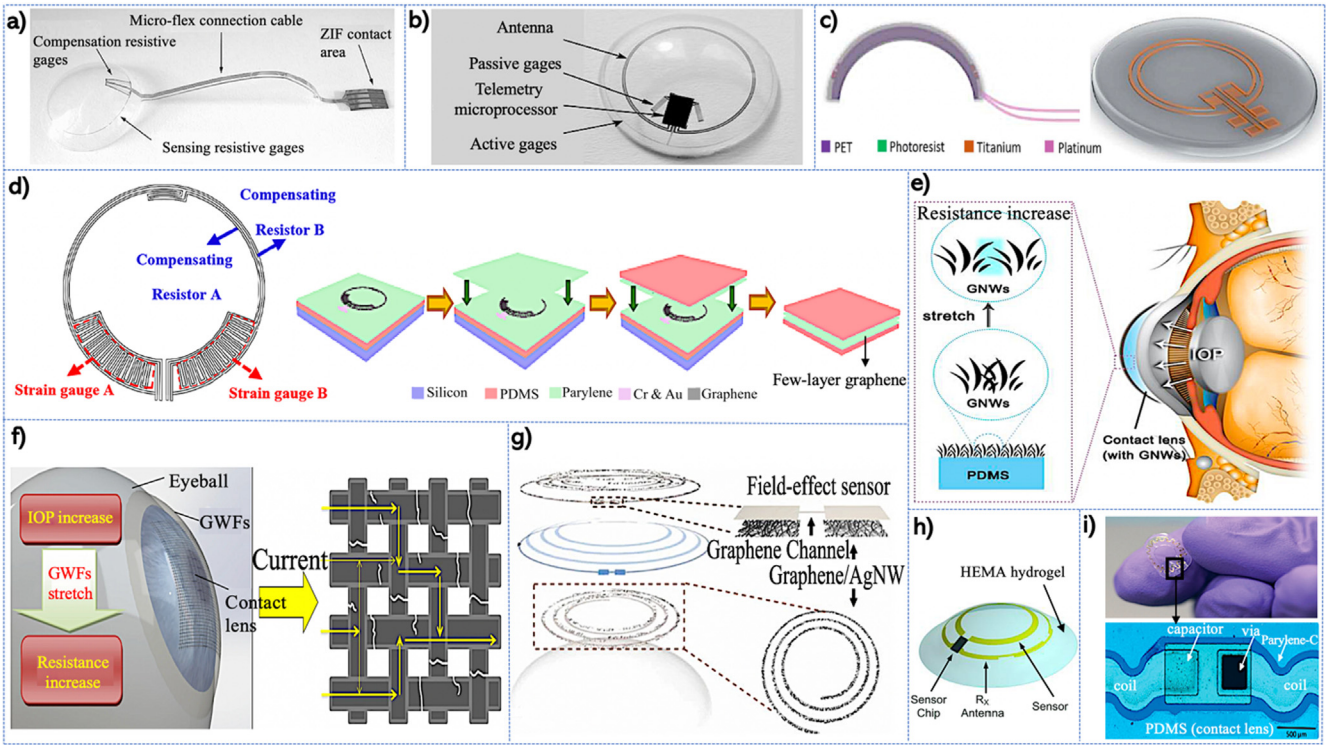

Fig. 6. Non-invasive MEMS contact lens pressure sensors. (**a**) A soft contact lens with an embedded microfabricated strain gauge. Wheatstone bridge circuit is used to eliminate the temperature drift for improved monitoring accuracy. Reproduced with permission from [43]. (**b**) The piezoresistive contact lens sensor with embedded telemetry microprocessor and antenna for wireless power and data transfer. Reproduced with permission from [44]. (**c**) A piezoresistive sensor with a metallic strain gauge on a transparent polyethylene terephthalate (PET) substrate. Reproduced with permission from [45]. (**d**) Graphene-based IOP device with Wheatstone bridge circuit. Reproduced with permission from [46]. (**e**) The piezoresistive IOP device using transparent graphene nanowalls (GNWs) for enhanced sensitivity. Reproduced with permission from [47]. (**f**) A contact lens tonometer with a fractured graphene woven fabric (GWF) monitors IOP with a high resolution. Reproduced with permission from [32]. (**g**) A multifunctional contact lens sensor with the graphene-silver nanowire (AgNW) hybrid nanostructure to simultaneously measure glucose and IOP levels with the independent electrical response. Reproduced with permission from [33]. (**h**) A wirelessly powered device with a capacitive sensor embedded in hydroxyethyl methacrylate (HEMA) contact lens to achieve a reconfigurable wide range and tunable sensitivity with a capacitance-to-digital converter (CDC). Reproduced with permission from [34]. (**i**) A soft, doughnut-shaped contact lens sensor with an embedded variable inductor and constant capacitor. Reproduced with permission from [35].

result in drift and instability because of the guide oil absorption and minuscule channel deformation. The former can be solved by using an oleophobic material (e.g., NOA65) to eliminate the absorption of oil and reducing channel width to increase stiffness addresses the latter. Compared to PDMS that has a high oleophilicity to cause a high absorption, Clearflex polyurethane absorbs significantly less than PDMS and NOA65 shows no absorption. Furthermore, the sensitivity of the NOA65 sensor increases linearly with the increasing number of rings for a liquid reservoir width of 50 μm, (e.g., 15.5 mm/% for a 5-ring sensor versus 4.5 mm/% for a single-ring sensor). The device performance is comparable to the commercial Tono-pen XL [40]. The follow-up work further explores a microfluidic signal filter to filter out rapid fluctuations (9 dB) from physiological noise (e.g., blinking) [83].

With a double spiral-shaped microchannel, a PDMS-based soft contact lens device has increased initial volume in the channel and decreased error in tracking fluid location (Fig. 5**d**) [41]. Placing the channel around the outer edge of the contact lens also leaves no obstruction to the visual field. As the curvature of the cornea changes, the volume of the embedded microchannel will change accordingly to displace the indicator fluid (avocado oil) in the channel to monitor IOP. The device shows a sensitivity of 40.8 μm/mmHg with a linearly responsive indicator position *ex vivo*. Another microfluidic IOP device monitor also relies on the movement of the dyed liquid in the deformed sensing chamber (Fig. 5**e**) [42]. The microfluidic contact lens sensor with an annular sensing chamber consists of a micropatterned soft elastomer sensing layer and a reference layer on hard plastic. The plastic-polyethylene terephthalate (PET) contact lens has PDMS at the inner surface to contact the cornea. *In vitro* test shows that the device sensitivity can be increased by either decreasing the cross-sectional area of the sensing channel or increasing the length of the annular distributed chamber. For instance, the decrease in the dimension of the sensing channel from 200 × 60 to 150 × 40 and then to 100 × 40 μm results in an increased sensitivity from 0.223 to 0.395 and then to 0.607 mm/mmHg for devices with the same diameter of 5.0 mm. After increasing the diameter to 8.5 mm, the sensitivity of the aforementioned three devices is further enhanced to 0.273, 0.474, and 0.708 mm/mmHg, respectively. The sensitivity of the device with a diameter of 5 mm and channel dimension of 150 × 40 μm is also observed to be 0.2832 mm/mmHg in the range of 8–32 mmHg *ex vivo*.

A polycarbonate film coated with a molecular metallic polycrystalline β -$(ET)_2I_3$ layer as a nanocomposite conducting bilayer can be embedded into a rigid, doughnut-shaped contact lens to yield a piezoresistive contact lens sensor with a sensitivity of 0.4 Ω/mmHg *in vivo* [84]. By using a Wheatstone bridge circuit composed of two metallic sensing resistive gauges for double sensitivity and another two for thermal compensation on a polyimide microflex substrate, the piezoresistive IOP device can further eliminate the temperature drift for enhanced accuracy (Fig. 6**a**) [43]. Although the device shows a sensitivity of 8.37 μV/mmHg in the range of 17–29 mmHg *in vitro*, it needs to be powered and wired for signal recording. To address this challenge, a follow-up work integrates a telemetry microprocessor and an antenna into the contact lens for wireless power and data transfer (Fig. 6**b**) [44]. The device shows a sensitivity of 113 μV/mmHg in 20–30 mmHg with high linearity of 0.9935 *ex vivo*.

The piezoresistive contact lens sensor with a Wheatstone bridge circuit can also be fabricated with a transparent PET (Fig. 6**c**) [45]. The device exhibits a sensitivity of 20 μV/mmHg in 9–30 mmHg with high linearity of 0.996 *in vitro*. However, this device still uses nontransparent Ti/Pt, which would block the visual field. Efforts to address this challenge leads to the use of highly transparent graphene (transparency of 97% for a single layer) [85] in the Wheatstone circuit bridge of the IOP device (Fig. 6**d**) [46]. Because the reduced initial resistance of the Wheatstone bridge circuit can increase the sensitivity, the increase in the number of graphene layers can help, but it lowers the transparency. Using few-layer graphene (3–5 layers) provides a trade-off, achieving a higher sensitivity of 150 μV/mmHg in 8–34 mmHg and a transparency of 85% *in vitro*.

Different from the metal-based contact lens sensors [44] that need to be patterned and positioned at the edge [43], the ones

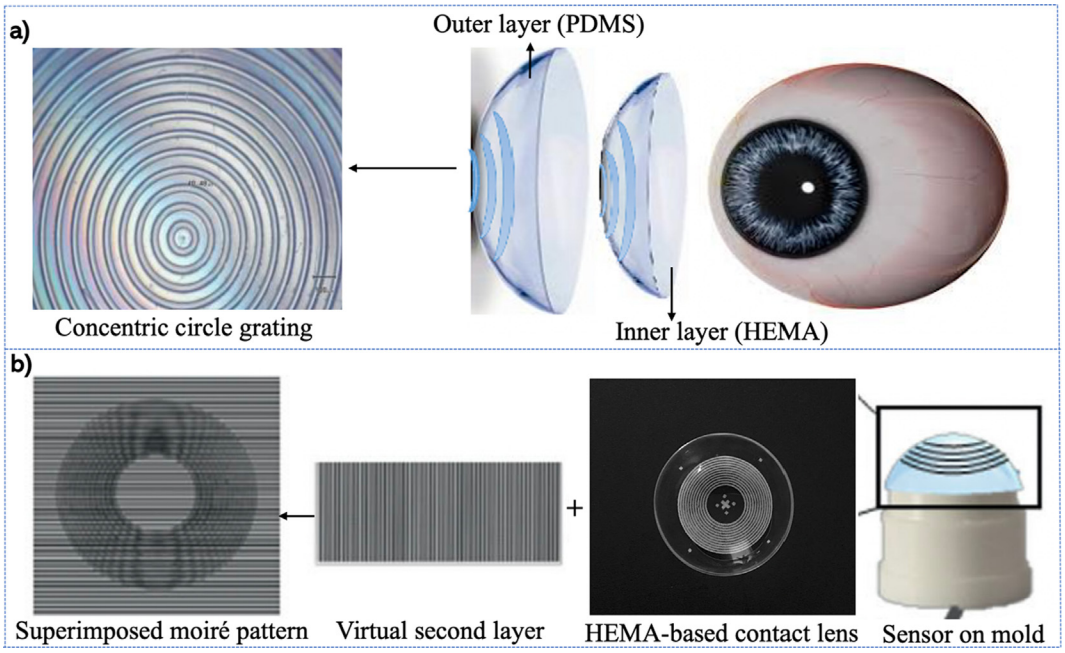

Fig. 7. Non-invasive optical contact lens pressure sensors. (**a**) A double-layer contact lens uses Moiré fringe patterns on the lens to detect IOP, where the inner HEMA layer can fit and bend with the cornea and the outer PDMS layer acts as a reference layer for generating moiré fringes. Reproduced with permission from [36]. (**b**) A moiré pattern-based contact lens sensor uses a computer-generated virtual image with the pattern printed on the HEMA contact lens. Reproduced with permission from [37].

based on a thin transparent membrane such as graphene nanowalls (GNWs) are attractive (sensitivity of 14.05 Ω/mmHg *in vitro*, Fig. 6**e)** [47]. The use of graphene woven fabric (GWF) in a contact lens tonometer also allows it to tightly attach to the cornea for IOP measurement with high resolution **(**Fig. 6**f)** [32]. Upon small deformation from IOP variation, high-density cracks appear in GWF to increase its resistance, which can be measured from the current for a constant voltage. The electrical resistance increase in GWF with the tensile strain is exponential with gauge factors of $\sim 10^3$ for strains of 2–6% and $\sim 10^6$ for higher strains [74]. Considering the high sensitivity, biocompatibility, and transparency (greater than80%), the resulting device exhibits a high sensitivity of 19.7 %/mmHg in 0–5 mmHg and 3.90 %/mmHg in 5–10 mmHg and a resolution of 6.8 %/mmHg in 0–10 mmHg *in vitro*.

With independent electrical responses, a soft, multifunctional contact lens can simultaneously measure IOP and glucose levels. Because the graphene-silver nanowire (AgNW) hybrid structure yields the stretchable and transparent electrode, it is used to result in a multifunctional contact lens with high transparency (greater than91%) and stretchability (∼25%) **(**Fig. 6**g)** [33]. The device shows a sensitivity of 2.64 MHz/mmHg in the range of 5–50 mmHg *in vitro*. A reconfigurable range and tunable sensitivity can also be achieved with a capacitive sensor embedded in a HEMA contact lens for a wirelessly powered device **(**Fig. 6**h)** [34]. The sensitivity and range can be simultaneously maximized with a capacitance-to-digital converter (CDC) that includes an integrator, a comparator, an analog signal generator, digital control circuits, and several capacitance arrays. An offset capacitor is applied for coarsely tuning the capacitor range, whereas a reference capacitor is used for sensitivity tuning the conversion gain. The device with a high sensitivity of 4.4 fF/mmHg, the low power consumption of 110 μW, and a large range of 2.25–30 mmHg (1.5–120 pF) compares favorably over the others in terms of power consumption and range (e.g., 1.4 mW with 5.3–5.75 pF [86] and 1.2 mW with 5–50 KΩ [87]). Besides design structures, sensitivity can also be modulated by the use of composite materials. A strain sensor fabricated with reduced graphene oxide @ polydopamine and silver nanoparticles @ carboxylated carbon nanotubes can achieve tunable sensitivity in a wide strain range up to 300% [88]. As a follow-up work of Fig. 3**g, a** non-invasive IOP pressure device is developed by replacing the commercial capacitor with a microfabricated one (while keeping the variable inductor and constant capacitor), which results in a soft, doughnut-shaped PDMS contact lens with a sensitivity of 35.1 kHz/mmHg *ex vivo* **(**Fig. 6**i)** [35].

Different from the integration of the pressure sensor in contact lens, a double-layer contact lens sensor can directly measure IOP by relating the moiré fringes pattern on the contact lens to the radius variation of the cornea **(**Fig. 7**a)** [36]. In the double-layer design, the inner hydrophilic HEMA layer can fit and bend with the circumference of the cornea, whereas the outer hydrophobic PDMS layer prevents sticking to the inner layer. Because of the preserved gap between the two layers, the deformed inner layer

Table 2
Comparison of sensor performance among various IOP monitoring devices

Type	Sensing performance (range, mmHg)	Fabrication material	Design structures	Ref
Piezo-resistive	8.37 μV[a] (17–29)[1]	PI, silicone	Wheatstone bridge circuit	[43]
	113 μV[a] (20–30)[3]	Pt/Ti, PI, silicone	Wheatstone bridge circuit	[44]
	20 μV[a] (9–30)[1]	Pt, PET	Wheatstone bridge circuit	[45]
	150 μV[a] (8–34)[1]	Graphene, PDMS	Wheatstone bridge circuit	[46]
	14.05 Ω[a] (N/A)[1]	GNWs, PDMS	GNWs assembled on contact lens	[47]
	19.7 %[a] (0–10)[2]	GWFs	GWFs bonded on contact lens	[32]
Capacitive	0.3 fF[a] (0–50)[3]	Ti/Au, parylene, LCP	Electrode sandwiched between layers	[14]
	0.12 pF[a] (10–21)[2]	Al, PI	Hollow mesa structure	[15]
	0.92 fF[a] (0–30)[4]	Si, Au, PEU, PDMS	Capsular tension ring-like structure	[26]
	4.4 fF[a] (2.25–30)[3]	Ti, Au, parylene, HEMA	Parallel-plate capacitor	[34]
Resonant	455 ppm[a] (N/A)[2]	Ti/Au, Si, SiO_2, parylene	Spiral inductor coil and parallel-plate capacitor embedded in diaphragm chamber	[16]
	542 ppm[a] (N/A)[4]	Ti/Au, parylene	Implantation tube attached to the backside of concentric sensing part	[17]
	156 kHz[a] (N/A)[4]	SU-8, parylene	Unique pressure reservoir	[18]
	4281 ppm[a] (0–60)[4]	Au, SU-8	Multipath circular spiral inductor	[19]
	1340 ppm[a] (0–50)[2]	PI, Cu, ferrite	Coil and capacitor on a membrane	[20]
	N/A (0–70)[4]	Ferrite, PI, Cu, Si	Two flexible membranes in inductor pattern	[21]
	57 kHz[a]/2667 kHz[a] (0–70)[3/4]	Ti, Cu, parylene	S-shaped inductor without sealed chamber	[22]
	15 kHz[a] (0–50)[1]	Si, SiO_2, Au, Cu, PI, stainless steel	Two-layer spiral coil, a capacitor, and an implantation needle	[23]
	3770 ppm[a] (0–60)[4]	Au, SU-8	Spiral inductive coil and a capacitor	[25]
	2.64 MHz[a] (5–50)[1]	AgNW, graphene, Ecoflex	Spiral coil	[33]
	35.1 kHz[a] (0–12.5)[3]	Ti, Au, PDMS, parylene	Doughnut-shaped contact lens with embedded capacitor and serpentine inductor	[35]
Optical	N/A (0–50)[4]	Al, Ag, PDMS	2-D nanophotonic grating structure	[24]
	1.2[b] (10–40)[4]	TiO_2, PDMS	Photonic crystal slab with an index layer on a periodically nanostructured surface	[28]
	0.6[b]/0.3[b] (5–45,0–60)[1/3]	SiN, SU-8	Cavity formed with a square diaphragm, rigid substrate, and a spacer	[27]
	1.3[b]/0.29[b] (0–40)[3/4]	Au, SiN, Si	Nanodot-embedded membrane on a reflective surface	[29]
	40 μm[a](N/A)[1]	HEMA, PDMS	Double-layer structure contact lens	[36]
	N/A (1–30)[2]	HEMA	Contact lens with a moiré pattern of concentric circles	[37]
Microfluidic	130 μm[a] (0–46)[4]	PDMS	Circular sensing chamber connected to sensing channels	[30]
	0.23 nm[a] (10–60)[3]	PC, PDMS, parylene	Microfluidic channel system with hydraulic amplification	[31]
	40.8 μm[a] (N/A)[3]	PDMS	Double spiral-shaped microchannel	[41]
	15.5 mm[a] (10–40)[3]	Silicone/hydrogel, NOA-65	Microfluidic dilatometer with liquid reservoir, air reservoir, and sensing channel	[40]
	0.2832 mm[a] (8–32)[3]	PET, PDMS	Annular sensing chamber: a micropatterned sensing layer and a hard reference layer	[42]

Note: sensitivity per mmHg [a] or accuracy [b]; Test conditions: *in vitro*[1], *in vivo*[2], *ex vivo*[3], and equipment[4].

can generate moiré fringes with the outer reference layer. A variation of 40 μm in the radius of artificial cornea corresponds to 1 mmHg pressure increment *in vitro*; thus, the number of the fringe varies to 6/7/7+/8 corresponding to 0/180/300/480 μm radius. However, the demonstrated sensitivity is not sufficient for practical use yet because the radius of the human cornea often varies 10–20 μm. Moreover, the design of two layers with increased thickness in the contact lens makes it uncomfortable for patients. A possible solution to bypass the double-layer structure is demonstrated in another moiré pattern-based IOP sensor with the use of a computer-generated virtual image **(**Fig. 7**b)** [37]. The concentric circle patterns are printed on a HEMA-based contact lens, whereas the other moiré pattern on a virtual second layer is generated by CAD software. Superimposed on the contact lens with virtual reference images, the device measures IOP in the range of 1–30 mmHg from the changes in a moiré pattern *in vivo* (Table 2).

2.3. Biomarker monitoring devices

Because of the large IOP fluctuation and its insufficient use for many early POAG patients, it is of high interest to explore POAG biomarkers for disease screening and therapy response monitoring. In addition to the ones in serum, aqueous humor (AH), vitreous body, or cerebrospinal fluid [89], tear also hosts glaucoma-related proteins directly from AH such as endothelin-1 [90], kallikrein and angiotensin [91], and Fas-mediated apoptosis [92]. The biomarkers to the inflammatory process induced by the drug can also be monitored, including proinflammatory cytokines [93], metalloproteinases (MMP) [94], and some autoantibody [95].

One of the most important biomarkers is cytokine (IL-12p70) because of its significant role related to RGC death and the pathogenesis of glaucoma [96]. A comparison of tear film between patients with early POAG and healthy individuals indicates its effectiveness as a new screening medium for glaucoma diagnosis. The mean concentration of IL-12p70 in tears of POAG patients is significantly lower than that from healthy counterparts (healthy: 3.94 ± 2.19 pg/ml vs. glaucoma: 2.31 ± 1.156 pg/ml) [97]. Induced by inflammatory cytokines, matrix- metalloproteinase-9 (MMP-9) is another AH biomarkers for the degenerative central nervous system (CNS) and eye disorders. Compared to the existing methods for tear sampling and biomarker analysis, wearable electronic devices can easily integrate biosensors into a contact lens to achieve the continuous detection of biomarkers (liquid biopsy).

A transparent anodic aluminum oxide (AAO) nanopore patterned thin film with a biomarker-specific antigen on the surface can be arranged in and around the central region of a PDMS-based contact lens to detect IL-12p70 (Fig. 8**a**) [38]. Upon biomarker binding, a change of the optical path difference occurs, so that a spectrometer can sense the shifts of optical signal reflected from the AAO film. The test in artificial tears shows a proportional shift from 1.2 to 9 nm as the concentration of biomarker increases from 0 to 10 pg/ml, indicating a sensitivity of 0.78 nm/(pg/ml). Moreover, this device with AAO nanopore structures can also measure IOP and deliver drugs. For instance, the film curvature changes from IOP variations can be measured from optical signal shifts, which shows a sensitivity of 0.02 nm/mmHg in 10–50 mmHg *ex vivo* comparable to the other IOP sensors [33]. The device also has high mechanical flexibility with no cracks in the AAO thin film after the 1000-cycle bending and stretching test.

Hydrogels have been widely used for biosensing [98,99], because of their high biocompatibility, antifouling, easy modification with label-free sensing probes (e.g., enzyme-degradable peptides), and anti-adsorption against non-specific proteins [100]. Because of better stability in diacrylamide-group-modified poly (ethyleneglycol) (PEG) diacrylamide (PEGDAAm) than PEG diacrylate, a fluorogenic IOL sensor (FIOL) with PEGDAAm hydrogel is designed to detect glaucoma biomarker MMP-9 **(**Fig. 8**b)** [39]. By adjusting hydrogel mesh size, a specific biomarker can selectively penetrate without diffusion of other cells or proteins. The hydrogel sensor demonstrates a dramatically enhanced fluorescence signal in the presence of MMP-9, with a LOD of 4.02 nM. Based on label-free detection, implanted semi-permanently in the eye, the FIOL can record the cumulative fluorescence signal induced by biomarkers for glaucoma progression. Compared to implantation with relatively rigid IOL, the flexible FIOL requires a smaller incision (~2.8 mm). Because of the slow diffusion of the injected MMP-9 inside the hydrogel to cleave peptide-probe, the dramatic increase of fluorescence signal is observed at day 43 post-injection *in vivo*. Considering the high turnover rate of AH and good FIOL/biomarker contact, it is beneficial to record the fluorescence signal in real-time. It should be noted that replacing the peptide sequence in the fluorogenic peptide probe with the target's specific

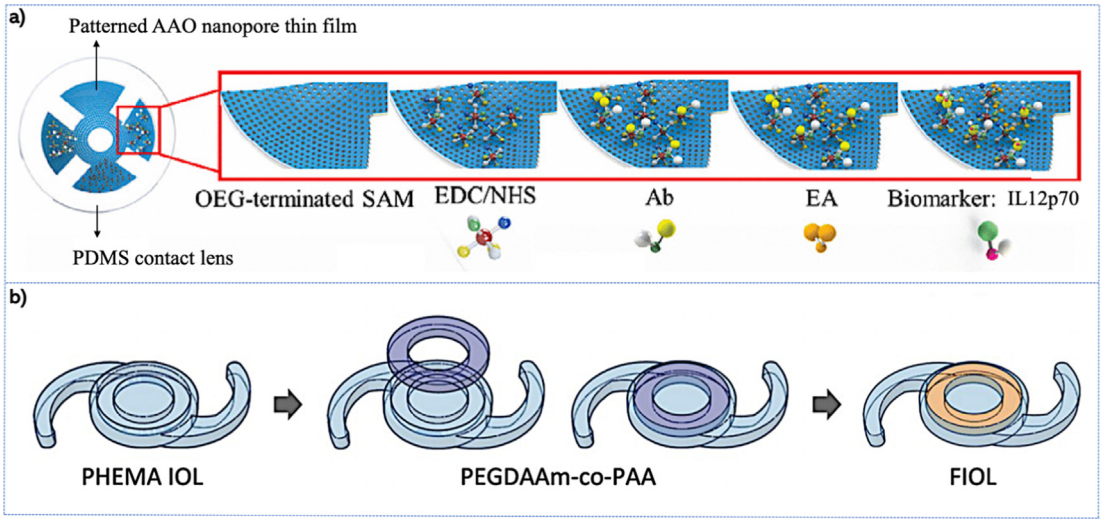

Fig. 8. Biomarker monitoring device. (a) A transparent anodic aluminum oxide (AAO) sensor with biomarker specific antigen on a PDMS-based contact lens can detect glaucoma-related biomarker IL-12p70. Once the biomarker binds to its antibody, the biomarker is detected by sensing optical signal shifts from the AAO film. Reproduced with permission from [38]. **(b)** An enzyme-activatable hydrogel-based fluorogenic IOL sensor can detect enzymatic biomarkers with the specific target peptide sequence at the fluorogenic peptide probe. The detection of MMP-9 is obtained from the fluorescence intensity. Reproduced with permission from [39].

one also allows its use for the detection of other enzymatic biomarkers.

3. Drug delivery devices for therapy

Several modes of ocular drug administration have been applied for glaucoma treatment, including systemic, topical, intravitreal, and periocular routes, where the topical installation is the relatively comfortable non-invasive method. Although topical ocular hypotensive medication is effective in delaying or preventing the POAG without a sign of glaucomatous damage [101], it is still difficult to maintain the required drug concentration at the targeted ocular tissue due to anatomical and physiological constraints of the eye [102]. Only less than 5% of topically applied formulation reaches the required site of action. The poor ocular bioavailability of topical formulation results from pre-corneal loss factors such as non-productive absorption, relative impermeability of the corneal epithelial membrane, transient residence time in the cul-de-sac, and tear dynamics [103]. As a result, extensive efforts focus on the analysis and design of new formulations to increase the residence time for enhanced permeation of ophthalmic drugs in the drug delivery system [104]. For example, nanosized formulations are developed to improve their ability to cross the anterior segment [105]. Permeation enhancers have also been added to various formulations such as solutions, emulsions, suspensions, and ointments. Furthermore, hydrogen has been identified as a promising therapeutic medical gas against glaucoma [106]. The evaluated IOP induces retinal ischemia–reperfusion (I/R) injury, which is closely related to the formation of reactive oxygen species (ROS), contributing to the pathogenesis of glaucomatous neurodegeneration [107]. By suppressing I/R induced oxidative stress, a continuous administration of hydrogen-loaded eyedrops can decrease retinal neuron apoptosis [108]. In addition to the improved drug ingredients, new encapsulation materials can also enhance the drug efficacy. For instance, timolol encapsulated by polyester microspheres allows delivery for more than 90 days *in vitro* [109]. Timolol maleate and brimonidine encapsulated by hybrid polyamidoamine dendrimer/ poly (lactic co-glycolic acid) nanoparticle can enable codelivery of the two drugs for a period of 28–35 days *in vitro*, which also effectively lowers IOP by 18% for 4 days *in vivo* [110]. The mesoporous silica nanoparticle can also encapsulate nitric oxide donors for glaucoma treatment, which reduces IOP up to 22% for 48 h *in vivo* [111]. Nevertheless, it is of high interest to develop drugs with enhanced ability to cross ocular barriers and with prolonged residence time for optimal drug concentration. The novel drug delivery systems are also important, including punctum plugs, subconjunctival/episcleral implants, cul-de-sac implants, and drug-eluting contact lenses.

The target for improved ophthalmic drug delivery includes longer ocular contact time, higher corneal permeability, or higher site-specificity [114]. Therefore, extensive efforts have been devoted to the development of colloidal suspension or viscous gel, application of inserts, and addition of polymers such as ethylene–vinyl acetate copolymer for prolonged drug retention in precorneal and increased bioavailability. Several approaches have also been applied to control the drug release system, including erodible (e.g., lacrisert, soluble ocular delivery implant and minidisc, nanoparticles and liposomes) and non-erodible methods (e.g., contact lenses, ocuserts, and diffusional inserts). For instance, an ocular insert made from hydrophilic and inert/zwitterionic polymers demonstrates the sustained and prolonged release of drugs without ocular irritation, as well as the enhanced ability to lower IOP compared to eyedrops [115].

Contact lenses with comfortability for extended wear are promising to deliver ocular drugs for multiple reasons. Firstly, contact lenses designed with a curved shape and thin surface to cover the cornea increase drug flux crossing the cornea with decreased drug inflow into to lacrimal duct for high bioavailability [116]. Secondly, because of the limited mixing between the fluid in the post-contact lens tear film and fluid outside this layer [117], the presence of a contact lens makes the drug molecules to contact with ocular tissue for extended release time. Therefore, ophthalmic drug delivery equipped with a contact lens requires less use of dose than topical ocular drops for efficient glaucoma treatment. There are mainly three types of contact lenses applied to drug delivery devices, namely soaking contact lens, particle-laden contact lens, and molecularly imprinted contact lens.

The efficiency of drug delivery from the soaking contact lens is higher than that by eyedrops [118]. Soaked to saturation in pilocarpine 1 percent, a hydrophilic contact lens made by vinyl pyrrolidone/acrylic copolymer with high water-content is applied for glaucoma treatment [119]. The soaking contact lens in 1 percent drug is as effective as eye drops with a 4 percent intensive medication *in vivo*. The drug penetration rate determined by the pore-size between the lattice structure and cross-linkages of the lens further allows modulation. The bioavailability of dexamethasone (DX) from a contact lens based on poly-2-hydroxyethyl methacrylate (PHEMA) is higher than eye drops [120]. Although more efficient than the direct use of topical eye drops, the soaking contact lens has inadequate drug loading and a short period of drug release. The challenge can be addressed by using particle-laden contact lenses or molecularly imprinted contact lenses.

The particle-laden contact lens entraps the drug in vesicles (e.g., nanoparticles, liposomes, and microemulsion) and then disperses from the contact lens. By dispersing lidocaine-loaded microemulsion drops or liposome in the particle-laden PHEMA contact lens, the release time is prolonged over 8 days for extended ocular drug delivery [121]. Similarly, a silicone hydrogel contact lens loaded with 5% timolol nanoparticles can extend the release time of timolol **(**Fig. 9**a)** [112]. Due to the trapped drugs in pores, a large portion of timolol will not release at a lower temperature (e.g., only 243 μg out of 316 μg released at 25C°). With refrigerated packaging, the gel can release the drug at therapeutic doses without an initial burst, which is also better to be stored in refrigerated conditions before wear. The drug delivery device releases timolol 5 μg/day for 20 days *in vivo*. A flexible nanopore thin-film device can simultaneously measure IOP and deliver the drug. The controlled drug release is achieved by storing drugs [PAA/GS/PAA/CHI] in a layer of a periodically distributed honeycomb-shape AAO nanopore designed with different diameters and depths for prolonged release time **(**Fig. 9**b)** [48]. With nanopores of 50 nm and 10 layers of [PAA/GS/PAA/CHI] coated on the nanopore thin film, the device shows drug release up to 15 days tested by flowing DI water through the device. Drug release time can be further extended by optimizing the nanopore size, porosity, and layers of [PAA/GS/PAA/CHI]. Similarly, the previously discussed example highlights a power-free device with an AAO nanopore thin film to real-time IOP measurement, biomarker detection, and in situ drug delivery **(**Fig. 9**c)** [38]. Facilitated by the hydrophilic surface of AAO thin film, the anti-glaucoma drug timolol mixed with a fluorescein dye solution can be easily loaded into the AAO nanopores. The in situ extended drug delivery of timolol has been shown to last up to 30 days.

The imprinted contact lens has two main advantages: controlled drug loading and delayed releasing [122]. The soft contact lens fabricated with molecular imprinting technology shows a larger timolol loading capacity than that of non-imprinted counterparts (34.7 μg versus 21.2 μg) and a higher concentration in tear fluid (2.0 and 3.0 fold higher than the non-imprinted and eyedrops) [123]. The molecularly imprinted hydrogel contact lenses also

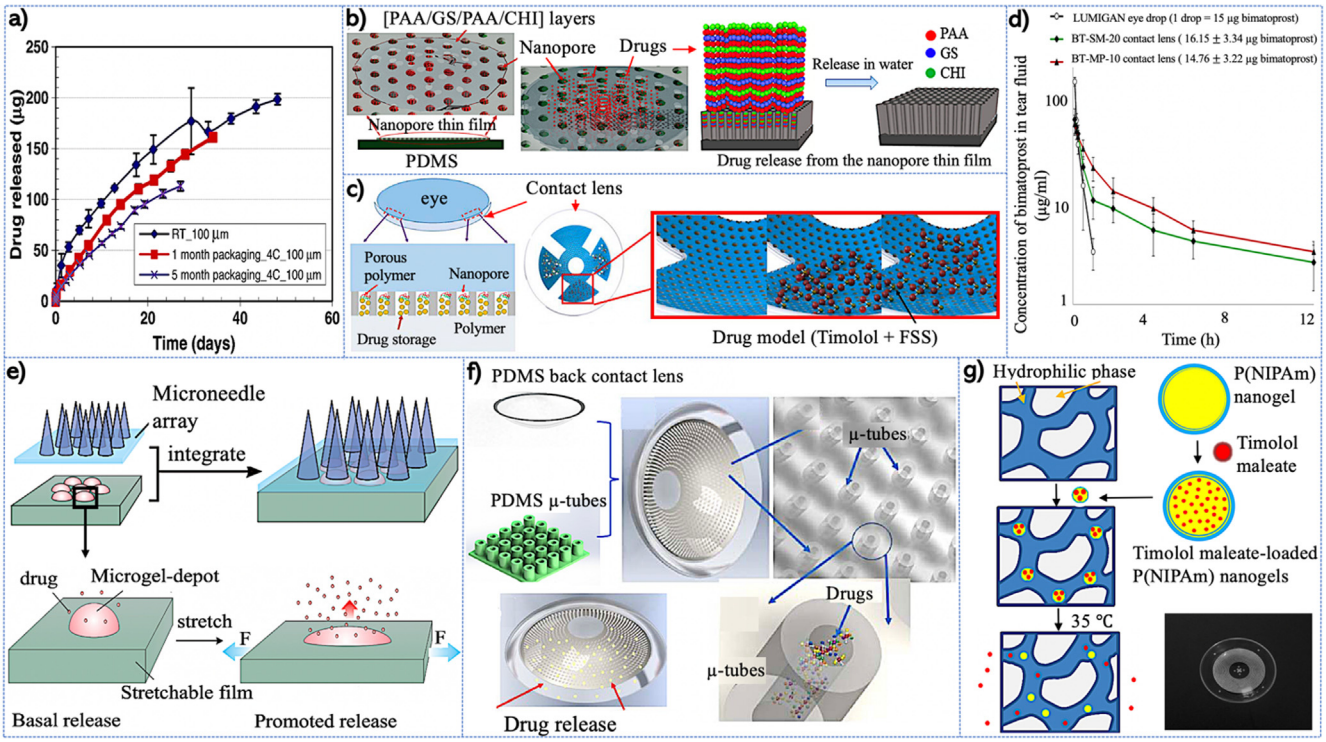

Fig. 9. Drug delivery devices for glaucoma. **(a)** A particle loaded silicone hydrogel used in the drug delivery device to extend the timolol release time. With refrigerated packaging, the gel can release the drug at a therapeutic dose without an initial burst. Reproduced with permission from [112]. **(b)** After storing drugs in the periodically distributed honeycomb-shape AAO nanopore, the nanopore thin-film device can extend the drug release time, with different diameters and depths to control drug release. Reproduced with permission from [48]. **(c)** The power-free device with the patterned AAO nanopore thin film contact lens for drug delivery with the hydrophilic surface of AAO film to facilitate the drug loading. Reproduced with permission from [38]. **(d)** The molecular imprinted contact lens shows an improved drug loading capacity, lower initial burst release, and prolonged retention time, compared to the soaking contact lens and eye drop solution. Reproduced with permission from [113]. **(e)** The micro depot follows the deformation of the stretchable elastomeric substrate upon stretching to facilitate the drug release from the micro depot. Reproduced with permission from [49]. **(f)** Microtubes (μ-tubes) as drug containers on the contact lens, with the change of their density and size to adjust the rate and time of drug release. Upon stretching, drug release becomes faster to indicate self-adaptive use. Reproduced with permission from [50]. **(g)** A body temperature-triggered drug delivery device based on a drug-eluting nanoporous contact lens with a polymerizable surfactant. Reproduced with permission from [37].

show zero-order (i.e., concentration independent) therapeutic release [124]. In addition to longer release time, the imprinted contact lens exhibits improved tear fluid bioavailability (e.g., 3 times greater than that from non-imprinted lenses) [125]. By imitating the natural receptors, bioinspired hydrogels in drug-eluting contact lenses generate binding sites to drug molecules for ocular drug delivery. With specific binding affinity, the molecularly imprinted contact lens with enhanced drug loading capacity can extend drug-release kinetics [126]. Compared to the soaking contact lens with a release rate of 58.3 ng/h for 24–36 h, bimatoprost imprinted silicone (HEMA) contact lens shows improved drug loading capacity and improved release kinetics (66.7 ng/h up to 36–60 h *in vitro*) for glaucoma treatment (Fig. 9**d**) [113]. The imprinted contact lens also shows a lower initial burst release of 56.26 μg/ml bimatoprost in tear fluid after 5 min wearing, as opposed to 145.26 μg/ml and 62.35 μg/ml from eye drop solution and the soaking contact lens, respectively. In contrast to a rapid fall in the drug concentration from eye drop solution, the other two have a prolonged retention time, and in particular, the imprinted one shows a relatively high drug concentration up to 12 h. The use of thicker drug-polymer films can enable a further sustained drug release time. For instance, a latanoprost-eluting contact lens [127] composed of poly (lactic-co-glycolic) acid (PLGA) with controlled drug release kinetics (approved for ocular and systemic drug delivery devices [128]) highlights a drug release for 4 weeks *in vivo*.

The glaucoma drug delivery in the contact lens triggered by the increased IOP can provide a more efficient, self-adaptive therapy in real-time; thus, the stimuli-triggered drug delivery system is of high interest [129]. Because of the potential for self-administration drug release, microgel depots containing drug-loaded nanoparticles in a stretchable silicone elastomer can promote drug release through microneedles arrays upon tensile strain [49] (Fig. 9**e**). The strain-triggered device shows a 2 folds higher release amount than that from the unstretched devices *in vitro*. Integrated with PDMS μ-tubes as drug containers, a contact lens drug delivery device can release the drug under diffusion, with both the release rate and time controlled by the density and size of the μ-tubes (Fig. 9**f**) [50]. The demonstration of the device highlights a prolonged drug release of up to 40 days with a higher bioavailability and lower risk of adverse effects. Based on the nanoporous contact lens using the timolol-loaded thermosensitive poly (N-isopropylacrylamide) (PNIPAM), the drug-eluting contact lens allows drug delivery triggered by the body temperature (Fig. 9**g**) [37]. After using the device for 3 h followed by drug release for up to 7 days, a high timolol concentration of 10.6 μg/ml appears in aqueous humor to result in a 33% decrease in IOP *in vivo* (timolol loaded in contact lens reduced from 507.23 to 2.65 μg).

4. Conclusion and future perspectives

This work summarizes the recent advancement of wearable electronic devices for glaucoma monitoring and therapy. Stretchable materials and structures, combined with electronics innovations, have resulted in improved device performance, including enhanced pressure sensitivity, extended sensing distance and mea-

surement range, lower power consumption, miniaturized device size, and higher biocompatibility. Besides fabrication materials and design structures, the implantation sites of the IOP devices also affect their sensing performance. The drug delivery systems also exhibit sustained drug release time, enhanced efficiency, and self-adaptive release, as well as controlled release rate and time. As one of the most important indicators, IOP can be measured with devices implanted to a specific site in the eye through minimally invasive implantation. The advantages and limitations of various commonly explored implanted locations have been discussed and compared, providing guidelines for the design and fabrication of IOP devices. After embedding pressure sensors into the contact lens or exploring the entire contact lens as the pressure sensor, the non-invasive measurement of IOP can be achieved. Although implantable IOP devices may provide more accurate measurements, the non-invasive IOP devices are more convenient to use. As for glaucoma therapy, different types of therapeutic contact lenses have also been explored to improve the efficiency of drug delivery systems. Triggered by IOP itself, self-adaptive drug delivery can be possible for more efficient therapy. Despite significant strides that have been made in glaucoma monitoring and therapy, challenges still exist to represent a small fraction of opportunities for future developments of devices to accurately detect onset and progression of glaucoma, which are briefly outlined as follows.

The IOP may not be homogeneous throughout the eye. The fundamental mechanisms of the IOP elevation and the consequent optic neuropathy are yet to be comprehensively investigated. Because eyeball temperature and swelling can also cause corneal curvature changes, the IOP pressure sensors are not sufficient, especially in the diagnosis of early POAG. Therefore, devices to detect biomarkers that complement IOP monitoring start to gain popularity. Although various biomarkers have been examined, opportunities still exist. For instance, diabetes mellitus (DM) is regarded as a risk factor related to POAG patients [130] and the relationship between DM and POAG is observed [131]. Therefore, the wide range of tear-based biosensors [132] to monitor glucose may also be leveraged to detect glaucoma-related biomarkers. Furthermore, a recent study indicates that the deformation of lamina cribrosa under elevated IOP uncovers the glaucomatous pathogenesis [133]. Nevertheless, the rapid progress of wearable electronic devices [134–136] provides a promising platform for continuous glaucoma monitoring and therapy, where the joint efforts from engineers and physicians are desirable in this interdisciplinary, burgeoning field.

CRediT authorship contribution statement

Wanqing Zhang: Conceptualization, Writing – original draft, Writing – review & editing. **Lingling Huang:** Writing – review & editing. **Robert N. Weinreb:** Writing – review & editing. **Huanyu Cheng:** Conceptualization, Resources, Writing – review & editing, Supervision.

Declaration of Competing Interest

RNW is consultant and Board member of Implandata and also consultant for IOPtic. Other authors declare that they have no known competing financial interests or personal relationships that could have appeared to influence the work reported in this paper.

Acknowledgments

H.C. would like to acknowledge the supports from the National Science Foundation (NSF) (Grant No. ECCS-1933072), the National Heart, Lung, and Blood Institute of the National Institutes of Health under Award Number R61HL154215, the Doctoral New Investigator grant from the American Chemical Society Petroleum Research Fund (59021-DNI7), and Penn State University. The partial support from the Center for Biodevices, the College of Engineering, and the Center for Security Research and Education at Penn State is also acknowledged. Also, supported in part by an unrestricted grant from Research to Prevent Blindness (New York, NY), and R01MD014850 from the National Institute on Minority Health and Health Disparities (R.N. W.).

References

[1] R.N. Weinreb, T. Aung, F.A. Medeiros, The pathophysiology and treatment of glaucoma: A review, JAMA - J. Am. Med. Assoc. 311 (2014) 1901–1911, https://doi.org/10.1001/jama.2014.3192.
[2] H. Quigley, A.T. Broman, The number of people with glaucoma worldwide in 2010 and 2020, Br. J. Ophthalmol. (2006), https://doi.org/10.1136/bjo.2005.081224.
[3] Y.-C. Tham, X. Li, T.Y. Wong, H.A. Quigley, T. Aung, C.-Y. Cheng, Global Prevalence of Glaucoma and Projections of Glaucoma Burden through 2040, Ophthalmology (2014), https://doi.org/10.1016/j.ophtha.2014.05.013.
[4] H.A. Quigley, 21st century glaucoma care, Eye. 33 (2) (2019) 254–260, https://doi.org/10.1038/s41433-018-0227-8.
[5] T. Realini, N. Weinreb, S. Wisniewski, Short-term repeatability of diurnal intraocular pressure patterns in glaucomatous individuals, Ophthalmology 118 (1) (2011) 47–51, https://doi.org/10.1016/j.ophtha.2010.04.027.
[6] T. Realini, R.N. Weinreb, S.R. Wisniewski, Diurnal intraocular pressure patterns are not repeatable in the short term in healthy individuals, Ophthalmology 117 (9) (2010) 1700–1704, https://doi.org/10.1016/j.ophtha.2010.01.044.
[7] J.H.K. Liu, R.P. Bouligny, D.F. Kripke, R.N. Weinreb, Nocturnal elevation of intraocular pressure is detectable in the sitting position, Investig. Ophthalmol. Vis. Sci. 44 (2003) 4439–4442, https://doi.org/10.1167/iovs.03-0349.
[8] J.H.K. Liu, D.F. Kripke, M.D. Twa, R.E. Hoffman, S.L. Mansberger, K.M. Rex, C.A. Girkin, R.N. Weinreb, Twenty-four-hour pattern of intraocular pressure in the aging population, Investig. Ophthalmol. Vis. Sci. 40 (1999) 2912–2917 (accessed April 29, 2021) https://europepmc.org/article/med/10549652.
[9] J.H.K. Liu, X. Zhang, D.F. Kripke, R.N. Weinreb, Twenty-four-hour intraocular pressure pattern associated with early glaucomatous changes, Investig. Ophthalmol. Vis. Sci. 44 (2003) 1586–1590, https://doi.org/10.1167/iovs.02-0666.
[10] Y. Barkana, S. Anis, J. Liebmann, C. Tello, R. Ritch, Clinical utility of intraocular pressure monitoring outside of normal office hours in patients with glaucoma, Arch. Ophthalmol. 124 (2006) 793–797, https://doi.org/10.1001/archopht.124.6.793.
[11] E.H. Hughes, P. Spry, J. Diamond, 24-Hour monitoring of intraocular pressure in glaucoma management: A retrospective review, in: J. Glaucoma, J Glaucoma, 2003: pp. 232–236. 10.1097/00061198-200306000-00009.
[12] Sensimed Triggerfish – Sensimed S.A., (n.d.). https://www.sensimed.ch/sensimed-triggerfish/ (accessed May 2, 2021).
[13] C. Wolfram, E. Stahlberg, N. Pfeiffer, Patient-reported nonadherence with glaucoma therapy, J. Ocul. Pharmacol. Ther. 35 (4) (2019) 223–228, https://doi.org/10.1089/jop.2018.0134.
[14] D. Ha, W.N. de Vries, S.W.M. John, P.P. Irazoqui, W.J. Chappell, Polymer-based miniature flexible capacitive pressure sensor for intraocular pressure (IOP) monitoring inside a mouse eye, Biomed. Microdevices 14 (1) (2012) 207–215, https://doi.org/10.1007/s10544-011-9598-3.
[15] F.G. Carrasco, D.D. Alonso, L. Niño-De-Rivera, Biocompatibility and implant of a less invasive intraocular pressure sensor, Microelectron. Eng. 159 (2016) 32–37, https://doi.org/10.1016/j.mee.2016.02.004.
[16] P.J. Chen, S. Saati, R. Varma, M.S. Humayun, Y.C. Tai, Wireless intraocular pressure sensing using microfabricated minimally invasive flexible-coiled LC sensor implant, J. Microelectromechanical Syst. (2010), https://doi.org/10.1109/JMEMS.2010.2049825.
[17] J.C.H. Lin, Y. Zhao, P.J. Chen, Y.C. Tai, High quality factor parylene-based intraocular pressure sensor, in: 2012 7th IEEE Int. Conf. Nano/Micro Eng. Mol. Syst. NEMS 2012, 2012: pp. 137–140. 10.1109/NEMS.2012.6196741.
[18] B. Crum, W. Li, Parylene-based fold-and-bond wireless pressure sensor, in: 8th Annu. IEEE Int. Conf. Nano/Micro Eng. Mol. Syst. IEEE NEMS 2013, 2013: pp. 1155–1158. 10.1109/NEMS.2013.6559926.
[19] B.A. Ganji, S.A. Kenari, S.S. Amiri, Increasing sensing distance of passive wireless IOP sensor, Microsyst. Technol. 25 (3) (2019) 887–896, https://doi.org/10.1007/s00542-018-4137-2.
[20] C.I. Jang, K.S. Shin, M.J. Kim, K.S. Yun, K.H. Park, J.Y. Kang, S.H. Lee, Effects of inner materials on the sensitivity and phase depth of wireless inductive pressure sensors for monitoring intraocular pressure, Appl. Phys. Lett. 108 (2016), https://doi.org/10.1063/1.4943136.
[21] B. Kang, H. Hwang, S.H. Lee, J.Y. Kang, J.-H. Park, C. Seo, C. Park, A wireless intraocular pressure sensor with variable inductance using a ferrite material, J. Semicond. Technol. Sci. 13 (4) (2013) 355–360, https://doi.org/10.5573/JSTS.2013.13.4.355.

[22] M.H.M. Kouhani, A. Weber, W. Li, Wireless intraocular pressure sensor using stretchable variable inductor, in: Proc. IEEE Int. Conf. Micro Electro Mech. Syst., Institute of Electrical and Electronics Engineers Inc., 2017: pp. 557–560. 10.1109/MEMSYS.2017.7863467.
[23] G. Chitnis, T. Maleki, B. Samuels, L.B. Cantor, B. Ziaie, A minimally invasive implantable wireless pressure sensor for continuous IOP monitoring, IEEE Trans. Biomed. Eng. 60 (1) (2013) 250–256, https://doi.org/10.1109/TBME.2012.2205248.
[24] Y.H. Kwon, J. Fernandes, J.-J. Kim, M.A. Croft, H. Liu, P.L. Kaufman, H. Jiang, Two-Dimensional Plasmonic Grating for Intraocular Pressure Sensing, IEEE Sensors Lett. 3 (10) (2019) 1–4, https://doi.org/10.1109/LSENS.778263410.1109/LSENS.2019.2942212.
[25] N. Xue, S.-P. Chang, J.-B. Lee, A SU-8-based microfabricated implantable inductively coupled passive RF wireless intraocular pressure sensor, J. Microelectromechanical Syst. 21 (6) (2012) 1338–1346, https://doi.org/10.1109/JMEMS.2012.2206072.
[26] Ç. Varel, Y.C. Shih, B.P. Otis, T.S. Shen, K.F. Böhringer, A wireless intraocular pressure monitoring device with a solder-filled microchannel antenna, J. Micromechanics Microengineering. 24 (2014), https://doi.org/10.1088/0960-1317/24/4/045012.
[27] A. Phan, P. Truong, J. Trumpp, F.E. Talke, Design of an optical pressure measurement system for intraocular pressure monitoring, IEEE Sens. J. 18 (1) (2018) 61–68, https://doi.org/10.1109/JSEN.2017.2767539.
[28] T. Karrock, M. Gerken, Pressure sensor based on flexible photonic crystal membrane, Biomed. Opt. Express 6 (2015) 4901, https://doi.org/10.1364/boe.6.004901.
[29] J.O. Lee, H. Park, J. Du, A. Balakrishna, O. Chen, D. Sretavan, H. Choo, A microscale optical implant for continuous in vivo monitoring of intraocular pressure, Microsystems Nanoeng. 3 (2017) 1–9, https://doi.org/10.1038/micronano.2017.57.
[30] J. Yan, An unpowered, wireless contact lens pressure sensor for point-of-care glaucoma diagnosis, in: Proc. Annu. Int. Conf. IEEE Eng. Med. Biol. Soc. EMBS, 2011: pp. 2522–2525. 10.1109/IEMBS.2011.6090698.
[31] B. Maeng, H.-K. Chang, J. Park, Photonic crystal-based smart contact lens for continuous intraocular pressure monitoring, Lab Chip 20 (10) (2020) 1740–1750, https://doi.org/10.1039/C9LC01268K.
[32] Y. Zhang, Y. Chen, T. Man, D. Huang, X. Li, H. Zhu, Z. Li, High resolution non-invasive intraocular pressure monitoring by use of graphene woven fabrics on contact lens, Microsystems Nanoeng. 5 (2019) 1–8, https://doi.org/10.1038/s41378-019-0078-x.
[33] J. Kim, M. Kim, M.S. Lee, K. Kim, S. Ji, Y.T. Kim, J. Park, K. Na, K.H. Bae, H.K. Kim, F. Bien, C.Y. Lee, J.U. Park, Wearable smart sensor systems integrated on soft contact lenses for wireless ocular diagnostics, Nat. Commun. 8 (2017), https://doi.org/10.1038/ncomms14997.
[34] J.C. Chiou, S.H. Hsu, Y.C. Huang, G.T. Yeh, W.T. Liou, C.K. Kuei, A wirelessly powered smart contact lens with reconfigurable wide range and tunable sensitivity sensor readout circuitry, Sensors (Switzerland). 17 (2017), https://doi.org/10.3390/s17010108.
[35] M.H. M. Kouhani, J. Wu, A. Tavakoli, A.J. Weber, W. Li, Wireless, passive strain sensor in a doughnut-shaped contact lens for continuous non-invasive self-monitoring of intraocular pressure, Lab Chip 20 (2) (2020) 332–342, https://doi.org/10.1039/C9LC00735K.
[36] P.C. Lin, C.S. Ho, L.A. Wang, I.J. Wang, J.Y. Yen, Intraocular Pressure Monitoring Using Moiré Patterns Generated from a Contact Lens, Japan Society of Applied Physics (2017), https://doi.org/10.7567/ssdm.2014.d-7-4.
[37] S.H. Lee, K.S. Shin, J.W. Kim, J.Y. Kang, J.K. Kim, Stimulus-responsive contact lens for IOP measurement or temperature-triggered drug release, Transl. Vis. Sci. Technol. 9 (2020) 1–1. 10.1167/tvst.9.4.1.
[38] C. Song, G. Ben-Shlomo, L. Que, A Multifunctional Smart Soft Contact Lens Device Enabled by Nanopore Thin Film for Glaucoma Diagnostics and in Situ Drug Delivery, J. Microelectromechanical Syst. 28 (5) (2019) 810–816, https://doi.org/10.1109/JMEMS.8410.1109/JMEMS.2019.2927232.
[39] M.K. Shin, Y.W. Ji, C.E. Moon, H. Lee, B. Kang, W.S. Jinn, J. Ki, B. Mun, M.H. Kim, H.K. Lee, S. Haam, Matrix metalloproteinase 9-activatable peptide-conjugated hydrogel-based fluorogenic intraocular-lens sensor, Biosens. Bioelectron. 162 (2020), https://doi.org/10.1016/j.bios.2020.112254 112254.
[40] S. Agaoglu, P. Diep, M. Martini, S. KT, M. Baday, I.E. Araci, Ultra-sensitive microfluidic wearable strain sensor for intraocular pressure monitoring, Lab Chip 18 (22) (2018) 3471–3483, https://doi.org/10.1039/C8LC00758F.
[41] A. Campigotto, Y. Lai, A Novel Non-invasive wearable sensor for Intraocular Pressure Measurement, Med. Devices Sensors. (2020) 1–10, https://doi.org/10.1002/mds3.10086.
[42] H. An, L. Chen, X. Liu, B. Zhao, H. Zhang, Z. Wu, Microfluidic contact lenses for unpowered, continuous and non-invasive intraocular pressure monitoring, Sensors Actuators, A Phys. 295 (2019) 177–187, https://doi.org/10.1016/j.sna.2019.04.050.
[43] M. Leonardi, P. Leuenberger, D. Bertrand, A. Bertsch, P. Renaud, First steps toward noninvasive intracular pressure monitoring with a sensing contact lens, Investig. Ophthalmol. Vis. Sci. (2004), https://doi.org/10.1167/iovs.04-0015.
[44] M. Leonardi, E.M. Pitchon, A. Bertsch, P. Renaud, A. Mermoud, Wireless contact lens sensor for intraocular pressure monitoring: assessment on enucleated pig eyes, Acta Ophthalmol. 87 (2009) 433–437, https://doi.org/10.1111/j.1755-3768.2008.01404.x.
[45] Y. Pang, Y. Li, X. Wang, C. Qi, Y. Yang, T.-L. Ren, A contact lens promising for non-invasive continuous intraocular pressure monitoring, RSC Adv. 9 (9) (2019) 5076–5082, https://doi.org/10.1039/C8RA10257K.
[46] J. Xu, T. Cui, T. Hirtz, Y. Qiao, X. Li, F. Zhong, X. Han, Y.i. Yang, S. Zhang, T.-L. Ren, Highly Transparent and Sensitive Graphene Sensors for Continuous and Non-invasive Intraocular Pressure Monitoring, ACS Appl. Mater. Interfaces 12 (16) (2020) 18375–18384, https://doi.org/10.1021/acsami.0c0299110.1021/acsami.0c02991.s001.
[47] Z. Liu, W. Pei, G. Wang, H. Chen, Three-Dimensional Graphene as Sensing Element for Intraocular Pressure Monitoring, in: Int. IEEE/EMBS Conf. Neural Eng. NER, IEEE Computer Society, 2019: pp. 803–806. 10.1109/NER.2019.8716899.
[48] C. Song, P. Deng, X. Ding, L. Que, A Flexible Nanopore Thin-Film-Enabled Device for Pressure Sensing and Drug Release, IEEE Trans. Nanotechnol. 17 (5) (2018) 962–967, https://doi.org/10.1109/TNANO.2018.2836322.
[49] J. Di, S. Yao, Y. Ye, Z. Cui, J. Yu, T.K. Ghosh, Y. Zhu, Z. Gu, Stretch-Triggered Drug Delivery from Wearable Elastomer Films Containing Therapeutic Depots, ACS Nano 9 (9) (2015) 9407–9415, https://doi.org/10.1021/acsnano.5b03975.
[50] X. DIng, C. Song, L. Que, Fabrication of Contact Lens Device with Integrated Microtubes for in Situ Extended Drug Delivery for Ocular Disease Treatment, in: 2019 20th Int. Conf. Solid-State Sensors, Actuators Microsystems Eurosensors XXXIII, TRANSDUCERS 2019 EUROSENSORS XXXIII, Institute of Electrical and Electronics Engineers Inc., 2019: pp. 306–309. 10.1109/TRANSDUCERS.2019.8808259.
[51] P.T. Khaw, A.R. Elkington, Glaucoma—1: Diagnosis, BMJ 328 (2004) 97, https://doi.org/10.1136/bmj.328.7431.97.
[52] J.T. Wilensky, Diurnal variations in intraocular pressure, in, Trans. Am. Ophthalmol. Soc. (1991).
[53] A.K.C. Lam, W.A. Douthwaite, The effect of an artificially elevated intraocular pressure on the central corneal curvature, Ophthalmic Physiol. Opt. 17 (1997) 18–24, https://doi.org/10.1016/S0275-5408(96)00033-6.
[54] A.V. Mantravadi, N. Vadhar, Glaucoma, Prim. Care - Clin. Off. Pract. 42 (3) (2015) 437–449, https://doi.org/10.1016/j.pop.2015.05.008.
[55] A.M. Shapero, Y. Liu, Y.C. Tai, Parylene-on-oil packaging for long-term implantable pressure sensors, Biomed. Microdevices 18 (2016) 1–10, https://doi.org/10.1007/s10544-016-0089-4.
[56] E. Chihara, Assessment of True Intraocular Pressure: The Gap Between Theory and Practical Data, Surv. Ophthalmol. (2008), https://doi.org/10.1016/j.survophthal.2008.02.005.
[57] R.L. Cooper, D.G. Beale, I.J. Constable, G.C. Grose, Continual monitoring of intraocular pressure: Effect of central venous pressure, respiration, and eye movements on continual recordings of intraocular pressure in the rabbit, dog, and man, Br. J. Ophthalmol. (1979), https://doi.org/10.1136/bjo.63.12.799.
[58] F.A. Medeiros, R.N. Weinreb, Evaluation of the influence of corneal biomechanical properties on intraocular pressure measurements using the ocular response analyzer, J. Glaucoma 15 (5) (2006) 364–370, https://doi.org/10.1097/01.ijg.0000212268.42606.97.
[59] T. Kida, J.H.K. Liu, R.N. Weinreb, Effect of 24-hour corneal biomechanical changes on intraocular pressure measurement, Investig. Ophthalmol. Vis. Sci. 47 (2006) 4422–4426, https://doi.org/10.1167/iovs.06-0507.
[60] V. Bhardwaj, G.P. Rajeshbhai, Axial length, anterior chamber depth-a study in different age groups and refractive errors, J. Clin. Diagnostic Res. (2013), https://doi.org/10.7860/JCDR/2013/7015.3473.
[61] J.A. Goldsmith, Y. Li, M.R. Chalita, V. Westphal, C.A. Patil, A.M. Rollins, J.A. Izatt, D. Huang, Anterior chamber width measurement by high-speed optical coherence tomography, Ophthalmology (2005), https://doi.org/10.1016/j.ophtha.2004.09.019.
[62] J. Park, J.K. Kim, S.J. Patil, J.K. Park, S.A. Park, D.W. Lee, A wireless pressure sensor integrated with a biodegradable polymer stent for biomedical applications, Sensors (Switzerland). (2016), https://doi.org/10.3390/s16060809.
[63] S. Melki, A. Todani, G. Cherfan, An implantable intraocular pressure transducer initial safety outcomes, JAMA Ophthalmol. 132 (2014) 1221–1225, https://doi.org/10.1001/jamaophthalmol.2014.1739.
[64] A. Shapero, A. Agarwal, J.C. Martinez, A. Emami, M.S. Humayun, Y.C. Tai, Wireless Implantable Intraocular Pressure Sensor with Parylene-Oil-Encapsulation and Forward-Angled RF Coil, Proc. IEEE Int. Conf. Micro Electro Mech. Syst. (2019) 21–24, https://doi.org/10.1109/MEMSYS.2019.8870787.
[65] O. Akar, T. Akin, K. Najafi, A wireless batch sealed absolute capacitive pressure sensor, Sensors Actuators, A Phys. 95 (2001) 29–38, https://doi.org/10.1016/S0924-4247(01)00753-1.
[66] P.J. Chen, S. Saati, R. Varma, M.S. Humayun, Y.C. Tai, Implantable flexible-coiled wireless intraocular pressure sensor, in: Proc. IEEE Int. Conf. Micro Electro Mech. Syst., 2009. 10.1109/MEMSYS.2009.4805364.
[67] G. Voskerician, M.S. Shive, R.S. Shawgo, H. Von Recum, J.M. Anderson, M.J. Cima, R. Langer, Biocompatibility and biofouling of MEMS drug delivery devices, Biomaterials (2003), https://doi.org/10.1016/S0142-9612(02)00565-3.
[68] T.V. Basova, E.S. Vikulova, S.I. Dorovskikh, A. Hassan, N.B. Morozova, The use of noble metal coatings and nanoparticles for the modification of medical implant materials, Mater. Des. 204 (2021), https://doi.org/10.1016/j.matdes.2021.109672 109672.
[69] S.H. Cho, H.M. Lu, L. Cauller, M.I. Romero-Ortega, J.B. Lee, G.A. Hughes, Biocompatible SU-8-based microprobes for recording neural spike signals

from regenerated peripheral nerve fibers, IEEE Sens. J. (2008), https://doi.org/10.1109/JSEN.2008.2006261.
[70] M.A. Croft, E. Lütjen-Drecoll, P.L. Kaufman, Age-related posterior ciliary muscle restriction – A link between trabecular meshwork and optic nerve head pathophysiology, Exp. Eye Res. (2017), https://doi.org/10.1016/j.exer.2016.07.007.
[71] A. Phan, P. Truong, A. Camp, K. Stewart, B. Suen, R.N. Weinreb, F.E. Talke, A Wireless Handheld Pressure Measurement System for in Vivo Monitoring of Intraocular Pressure in Rabbits, IEEE Trans. Biomed. Eng. 67 (3) (2020) 931–937, https://doi.org/10.1109/TBME.1010.1109/TBME.2019.2924440.
[72] P.C. Hui, K. Shtyrkova, C. Zhou, X. Chen, J. Chodosh, C.H. Dohlman, E.I. Paschalis, Implantable self-aligning fiber-optic optomechanical devices for in vivo intraocular pressure-sensing in artificial cornea, J. Biophotonics 13 (2020) 1–13, https://doi.org/10.1002/jbio.202000031.
[73] J.O. Lee, V. Narasimhan, J. Du, B. Ndjamen, D. Sretavan, H. Choo, Biocompatible Multifunctional Black-Silicon for Implantable Intraocular Sensor, Adv. Healthc. Mater. (2017), https://doi.org/10.1002/adhm.201601356.
[74] K. Mansouri, F.A. Medeiros, A. Tafreshi, R.N. Weinreb, Continuous 24-hour monitoring of intraocular pressure patterns with contact lens sensor: Safety, tolerability, and reproducibility in patients with glaucoma, Arch. Ophthalmol. 130 (2012) 1534–1539, https://doi.org/10.1001/archophthalmol.2012.2280.
[75] T. Takamatsu, Y. Chen, T. Yoshimasu, M. Nishizawa, T. Miyake, Highly Efficient, Flexible Wireless-Powered Circuit Printed on a Moist, Soft Contact Lens, Adv. Mater. Technol. (2019), https://doi.org/10.1002/admt.201800671.
[76] B. Nuyen, K. Mansouri, Detecting IOP Fluctuations in Glaucoma Patients, Open Ophthalmol. J. 10 (1) (2016) 44–55, https://doi.org/10.2174/1874364101610010044.
[77] M. Nasreldin, R. Delattre, M. Ramuz, C. Lahuec, T. Djenizian, J.L. De Bougrenet De la Tocnaye, Flexible micro-battery for powering smart contact lens, Sensors (Switzerland). (2019). 10.3390/s19092062.
[78] J.C. Lin, A new IEEE standard for safety levels with respect to human exposure to radio-frequency radiation, IEEE Antennas Propag. Mag. (2006), https://doi.org/10.1109/MAP.2006.1645601.
[79] J. Park, D.B. Ahn, J. Kim, E. Cha, B.S. Bae, S.Y. Lee, J.U. Park, Printing of wirelessly rechargeable solid-state supercapacitors for soft, smart contact lenses with continuous operations, Sci. Adv. 5 (2019) 1–9, https://doi.org/10.1126/sciadv.aay0764.
[80] H.W. Cheng, B.M. Jeng, C.Y. Chen, H.Y. Huang, J.C. Chiou, C.H. Luo, The rectenna design on contact lens for wireless powering of the active intraocular pressure monitoring system, Proc. Annu. Int. Conf. IEEE Eng. Med. Biol. Soc. EMBS. (2013) 3447–3450, https://doi.org/10.1109/EMBC.2013.6610283.
[81] A.R. Lingley, M. Ali, Y. Liao, R. Mirjalili, M. Klonner, M. Sopanen, S. Suihkonen, T. Shen, B.P. Otis, H. Lipsanen, B.A. Parviz, A single-pixel wireless contact lens display, J. Micromechanics Microengineering. 21 (2011), https://doi.org/10.1088/0960-1317/21/12/125014.
[82] M. Yuan, R. Das, R. Ghannam, Y. Wang, J. Reboud, R. Fromme, F. Moradi, H. Heidari, Electronic Contact Lens: A Platform for Wireless Health Monitoring Applications, Adv. Intell. Syst. 2 (2020) 1900190, https://doi.org/10.1002/aisy.201900190.
[83] I. Emre Araci, Sevda Agaoglu, Ju Young Lee, Laura Rivas Yepes, Priscilla Diep, Matthew Martini, Andrew Schmidt, Flow stabilization in wearable microfluidic sensors enables noise suppression, Lab Chip 19 (22) (2019) 3899–3908, https://doi.org/10.1039/C9LC00842J.
[84] I. Sánchez, V. Laukhin, A. Moya, R. Martin, F. Ussa, E. Laukhina, A. Guimera, R. Villa, C. Rovira, J. Aguiló, J. Veciana, J.C. Pastor, Prototype of a nanostructured sensing contact lens for noninvasive intraocular pressure monitoring, Investig. Ophthalmol. Vis. Sci. 52 (2011) 8310–8315, https://doi.org/10.1167/iovs.10-7064.
[85] F. Bonaccorso, Z. Sun, T. Hasan, A.C. Ferrari, Graphene photonics and optoelectronics, Nat. Photonics (2010), https://doi.org/10.1038/nphoton.2010.186.
[86] Eric Y. Chow, Arthur L. Chlebowski, Pedro P. Irazoqui, A miniature-implantable RF-wireless active glaucoma intraocular pressure monitor, in, IEEE Trans. Biomed. Circuits Syst. 4 (6) (2010) 340–349, https://doi.org/10.1109/TBCAS.2010.2081364.
[87] A. Donida, G. Di Dato, P. Cunzolo, M. Sala, F. Piffaretti, P. Orsatti, D. Barrettino, A Circadian and Cardiac Intraocular Pressure Sensor for Smart Implantable Lens, IEEE Trans. Biomed. Circuits Syst. (2015), https://doi.org/10.1109/TBCAS.2015.2501320.
[88] S. Zhao, P. Zheng, Q. Liu, L. Niu, H. Cong, A. Wan, Highly stretchable strain sensor with tunable sensitivity via polydopamine template-assisted dual-mode cooperative conductive network for human motion detection, Mater. Des. (2021), https://doi.org/10.1016/j.matdes.2021.109780 109780.
[89] L. Agnifili, D. Pieragostino, A. Mastropasqua, V. Fasanella, L. Brescia, G.M. Tosi, P. Sacchetta, L. Mastropasqua, Molecular biomarkers in primary open-angle glaucoma: From noninvasive to invasive, Prog. Brain Res. (2015), https://doi.org/10.1016/bs.pbr.2015.05.006.
[90] L. Choritz, M. Machert, H. Thieme, Correlation of endothelin-1 concentration in aqueous humor with intraocular pressure in primary open angle and pseudoexfoliation glaucoma, Investig. Ophthalmol. Vis. Sci. (2012), https://doi.org/10.1167/iovs.12-10216.
[91] D. Borovic, E. Bendelic, D. Chiseliță, Study of kini-kallikrein and renin–angiotensin systems in patients with primary open angle glaucoma, Oftalmologia (2009).
[92] O.S. Slepova, M.A. Frolov, N.S. Morozova, A.M. Frolov, D.N. Lovpache, Markers of Fas-mediated apoptosis in primary open-angle glaucoma and opportunities of their pharmacological correction, Vestn. oftalmol. 128 (2012) 27–31 (accessed April 30, 2021) https://europepmc.org/article/med/22994104.
[93] L. Malvitte, T. Montange, A. Vejux, C. Baudouin, A.M. Bron, C. Creuzot-Garcher, G. Lizard, Measurement of inflammatory cytokines by multicytokine assay in tears of patients with glaucoma topically treated with chronic drugs, Br. J. Ophthalmol. 91 (1) (2007) 29–32, https://doi.org/10.1136/bjo.2006.101485.
[94] Hae-Young Lopilly Park, Jie Hyun Kim, Kyung Min Lee, Chan Kee Park, Effect of prostaglandin analogues on tear proteomics and expression of cytokines and matrix metalloproteinases in the conjunctiva and cornea, Exp. Eye Res. 94 (1) (2012) 13–21, https://doi.org/10.1016/j.exer.2011.10.017.
[95] F.H. Grus, V.N. Podust, K. Bruns, K. Lackner, S. Fu, E.A. Dalmasso, A. Wirthlin, N. Pfeiffer, SELDI-TOF-MS ProteinChip array profiling of tears from patients with dry eye, Investig. Ophthalmol. Vis. Sci. (2005), https://doi.org/10.1167/iovs.04-0448.
[96] R. Vohra, J.C. Tsai, M. Kolko, The Role of Inflammation in the Pathogenesis of Glaucoma, Surv. Ophthalmol. (2013), https://doi.org/10.1016/j.survophthal.2012.08.010.
[97] D. Gupta, J.C. Wen, J.L. Huebner, S. Stinnett, V.B. Kraus, H.C. Tseng, M. Walsh, Cytokine biomarkers in tear film for primary open-angle glaucoma, Clin. Ophthalmol. 11 (2017) 411–416, https://doi.org/10.2147/OPTH.S125364.
[98] K. Zhang, J. Li, J. Jin, J. Dong, L. Li, B. Xue, W. Wang, Q. Jiang, Y. Cao, Injectable, anti-inflammatory and conductive hydrogels based on graphene oxide and diacerein-terminated four-armed polyethylene glycol for spinal cord injury repair, Mater. Des. 196 (2020), https://doi.org/10.1016/j.matdes.2020.109092 109092.
[99] Z. Huang, C. Gao, Y. Huang, X. Zhang, X. Deng, Q. Cai, X. Yang, Injectable polyphosphazene/gelatin hybrid hydrogel for biomedical applications, Mater. Des. 160 (2018) 1137–1147, https://doi.org/10.1016/j.matdes.2018.11.010.
[100] J.A. Benton, B.D. Fairbanks, K.S. Anseth, Characterization of valvular interstitial cell function in three dimensional matrix metalloproteinase degradable PEG hydrogels, Biomaterials (2009), https://doi.org/10.1016/j.biomaterials.2009.08.031.
[101] M.O. Gordon, J.A. Beiser, J.D. Brandt, D.K. Heuer, E.J. Higginbotham, C.A. Johnson, J.L. Keltner, J. Philip Miller, R.K. Parrish, M. Roy Wilson, M.A. Kass, The Ocular Hypertension Treatment Study: Baseline factors that predict the onset of primary open-angle glaucoma, Arch. Ophthalmol. 120 (2002) 714–720. 10.1001/archopht.120.6.714.
[102] John C. Lang, Ocular drug delivery conventional ocular formulations, Adv. Drug Deliv. Rev. 16 (1) (1995) 39–43, https://doi.org/10.1016/0169-409X(95)00012-V.
[103] A. Urtti, L. Salminen, Minimizing systemic absorption of topically administered ophthalmic drugs, Surv. Ophthalmol. (1993), https://doi.org/10.1016/0039-6257(93)90141-S.
[104] N. Nagai, Design of novel ophthalmic formulation containing drug nanoparticles and its usefulness as anti-glaucoma drugs, Yakugaku Zasshi (2016), https://doi.org/10.1248/yakushi.16-00089.
[105] D.R. Janagam, L. Wu, T.L. Lowe, Nanoparticles for drug delivery to the anterior segment of the eye, Adv. Drug Deliv. Rev. (2017), https://doi.org/10.1016/j.addr.2017.04.001.
[106] Y. Tao, L. Geng, W.W. Xu, L.M. Qin, G.H. Peng, Y.F. Huang, The potential utilizations of hydrogen as a promising therapeutic strategy against ocular diseases, Ther. Clin. Risk Manag. 12 (2016) 799–806, https://doi.org/10.2147/TCRM.S102518.
[107] G. Tezel, Oxidative stress in glaucomatous neurodegeneration: Mechanisms and consequences, Prog. Retin. Eye Res. (2006), https://doi.org/10.1016/j.preteyeres.2006.07.003.
[108] H. Oharazawa, T. Igarashi, T. Yokota, H. Fujii, H. Suzuki, M. Machide, H. Takahashi, S. Ohta, I. Ohsawa, Protection of the retina by rapid diffusion of hydrogen: Administration of hydrogen-loaded eye drops in retinal ischemia-reperfusion injury, Investig. Ophthalmol. Vis. Sci. (2010), https://doi.org/10.1167/iovs.09-4089.
[109] J.P. Bertram, S.S. Saluja, J. McKain, E.B. Lavik, Sustained delivery of timolol maleate from poly(lactic-co-glycolic acid)/ poly(lactic acid) microspheres for over 3 months, J. Microencapsul. (2009), https://doi.org/10.1080/02652040802095250.
[110] Hu Yang, Puneet Tyagi, Rajendra S. Kadam, Christopher A. Holden, Uday B. Kompella, Hybrid dendrimer hydrogel/PLGA nanoparticle platform sustains drug delivery for one week and antiglaucoma effects for four days following one-time topical administration, ACS Nano 6 (9) (2012) 7595–7606, https://doi.org/10.1021/nn301873v.
[111] C. Hu, J. Sun, Y. Zhang, J. Chen, Y. Lei, X. Sun, Y. Deng, Local Delivery and Sustained-Release of Nitric Oxide Donor Loaded in Mesoporous Silica Particles for Efficient Treatment of Primary Open-Angle Glaucoma, Adv. Healthc. Mater. 7 (2018) 1–10, https://doi.org/10.1002/adhm.201801047.
[112] Hyun Jung Jung, Michelle Abou-Jaoude, Blanca E. Carbia, Caryn Plummer, Anuj Chauhan, Glaucoma therapy by extended release of timolol from nanoparticle loaded silicone-hydrogel contact lenses, J. Control. Release 165 (1) (2013) 82–89, https://doi.org/10.1016/j.jconrel.2012.10.010.

[113] F. Yan, Y. Liu, S. Han, Q. Zhao, N. Liu, Bimatoprost Imprinted Silicone Contact Lens to Treat Glaucoma, AAPS PharmSciTech. (2020), https://doi.org/10.1208/s12249-020-1622-6.
[114] N. Gulati, V. Dwivedi, Review on Ocular Drug Delivery System and Its Devices, Int. J. Drug Regul. Aff. 2 (2018) 79–82. 10.22270/ijdra.v2i3.145.
[115] Prakash Bhagav, Vaibhav Trivedi, Darshan Shah, Sajeev Chandran, Sustained release ocular inserts of brimonidine tartrate for better treatment in open-angle glaucoma, Drug Deliv, Transl. Res. 1 (2) (2011) 161–174, https://doi.org/10.1007/s13346-011-0018-2.
[116] Himanshu Gupta, Mohammed Aqil, Contact lenses in ocular therapeutics, Drug Discov. Today. 17 (9-10) (2012) 522–527, https://doi.org/10.1016/j.drudis.2012.01.014.
[117] F.A. Maulvi, T.G. Soni, D.O. Shah, A review on therapeutic contact lenses for ocular drug delivery, Drug Deliv. (2016), https://doi.org/10.3109/10717544.2016.1138342.
[118] Chi-Chung Li, Anuj Chauhan, Modeling ophthalmic drug delivery by soaked contact lenses, Ind. Eng. Chem. Res. 45 (10) (2006) 3718–3734, https://doi.org/10.1021/ie0507934.
[119] J S Hillman, Management of acute glaucoma with Pilocarpine soaked hydrophilic lens, Br. J. Ophthalmol. 58 (7) (1974) 674–679, https://doi.org/10.1136/bjo.58.7.674.
[120] J. Kim, A. Chauhan, Dexamethasone transport and ocular delivery from poly (hydroxyethyl methacrylate) gels, Int. J. Pharm. 353 (2008) 205–222, https://doi.org/10.1016/j.ijpharm.2007.11.049.
[121] D. Gulsen, A. Chauhan, Dispersion of microemulsion drops in HEMA hydrogel: A potential ophthalmic drug delivery vehicle, Int. J. Pharm. (2005), https://doi.org/10.1016/j.ijpharm.2004.11.033.
[122] C.J. White, M.E. Byrne, Molecularly imprinted therapeutic contact lenses, Expert Opin. Drug Deliv. (2010), https://doi.org/10.1517/17425241003770098.
[123] Haruyuki Hiratani, Akihito Fujiwara, Yuka Tamiya, Yuri Mizutani, Carmen Alvarez-Lorenzo, Ocular release of timolol from molecularly imprinted soft contact lenses, Biomaterials 26 (11) (2005) 1293–1298, https://doi.org/10.1016/j.biomaterials.2004.04.030.
[124] Maryam Ali, Shin Horikawa, Siddarth Venkatesh, Jishnu Saha, Jong Wook Hong, Mark E. Byrne, Zero-order therapeutic release from imprinted hydrogel contact lenses within in vitro physiological ocular tear flow, J. Control. Release 124 (3) (2007) 154–162, https://doi.org/10.1016/j.jconrel.2007.09.006.
[125] A. Tieppo, C.J. White, A.C. Paine, M.L. Voyles, M.K. McBride, M.E. Byrne, Sustained in vivo release from imprinted therapeutic contact lenses, J. Control. Release (2012), https://doi.org/10.1016/j.jconrel.2011.09.087.
[126] C. Alvarez-Lorenzo, S. Anguiano-Igea, A. Varela-García, M. Vivero-Lopez, A. Concheiro, Bioinspired hydrogels for drug-eluting contact lenses, Acta Biomater. (2019), https://doi.org/10.1016/j.actbio.2018.11.020.
[127] J.B. Ciolino, C.F. Stefanescu, A.E. Ross, B. Salvador-Culla, P. Cortez, E.M. Ford, K. A. Wymbs, S.L. Sprague, D.R. Mascoop, S.S. Rudina, S.A. Trauger, F. Cade, D.S. Kohane, Invivo performance of a drug-eluting contact lens to treat glaucoma for a month, Biomaterials 35 (2014) 432–439, https://doi.org/10.1016/j.biomaterials.2013.09.032.
[128] R.A. Jain, The manufacturing techniques of various drug loaded biodegradable poly(lactide-co-glycolide) (PLGA) devices, Biomaterials (2000), https://doi.org/10.1016/S0142-9612(00)00115-0.
[129] Y. Wang, M.S. Shim, N.S. Levinson, H.W. Sung, Y. Xia, Stimuli-responsive materials for controlled release of theranostic agents, Adv. Funct. Mater. (2014), https://doi.org/10.1002/adfm.201400279.
[130] S.Y. Rhee, Y.C. Hwang, H.Y. Chung, J.T. Woo, Vitamin D and diabetes in Koreans: Analyses based on the Fourth Korea National Health and Nutrition Examination Survey (KNHANES), 2008–2009, Diabet. Med. 29 (2012) 1003–1010, https://doi.org/10.1111/j.1464-5491.2012.03575.x.
[131] M. Zhou, W. Wang, W. Huang, X. Zhang, Diabetes mellitus as a risk factor for open-angle glaucoma: A systematic review and meta-analysis, PLoS ONE 9 (2014), https://doi.org/10.1371/journal.pone.0102972.
[132] A. Sheng, L. Lin, J. Zhu, J. Zhuang, J. Li, L. Chang, H. Cheng, Micro/nanodevices for assessment and treatment in stomatology and ophthalmology, Microsystems Nanoeng. 7 (2021) 1–19, https://doi.org/10.1038/s41378-021-00238-1.
[133] L. Li, F. Song, Biomechanical research of lamina cribrosa in glaucoma, Natl. Sci. Rev. (2020), https://doi.org/10.1093/nsr/nwaa063.
[134] Ling Zhang, Hongjun Ji, Houbing Huang, Ning Yi, Xiaoming Shi, Senpei Xie, Yaoyin Li, Ziheng Ye, Pengdong Feng, Tiesong Lin, Xiangli Liu, Xuesong Leng, Mingyu Li, Jiaheng Zhang, Xing Ma, Peng He, Weiwei Zhao, Huanyu Cheng, Wearable Circuits Sintered at Room Temperature Directly on the Skin Surface for Health Monitoring, ACS Appl. Mater. Interfaces 12 (40) (2020) 45504–45515, https://doi.org/10.1021/acsami.0c1147910.1021/acsami.0c11479.s001.
[135] H. Zhou, Y. Zhang, Y. Qiu, H. Wu, W. Qin, Y. Liao, Q. Yu, H. Cheng, Stretchable piezoelectric energy harvesters and self-powered sensors for wearable and implantable devices, Biosens. Bioelectron. 168 (2020), https://doi.org/10.1016/j.bios.2020.112569 112569.
[136] J. Zhu, Z. Hu, C. Song, N. Yi, Z. Yu, Z. Liu, S. Liu, M. Wang, M.G. Dexheimer, J. Yang, H. Cheng, Stretchable wideband dipole antennas and rectennas for RF energy harvesting, Mater. Today Phys. 18 (2021), https://doi.org/10.1016/j.mtphys.2021.100377 100377.